4-17-2012 12:00 AM

Bubble-free oxygen and carbon dioxide mass transfer in bioreactors using microporous membranes

Ravi Balgobin
The University of Western Ontario

Supervisor
Dr. Dimitre Karamanev
The University of Western Ontario

Graduate Program in Chemical and Biochemical Engineering
A thesis submitted in partial fulfillment of the requirements for the degree in Master of Engineering Science

BUBBLE-FREE OXYGEN AND CARBON DIOXIDE MASS TRANSFER IN BIOREACTORS USING MICROPOROUS MEMBRANES

(Spine title: Bubble-free membrane gas transfer in bioreactors)

(Thesis format: Monograph)

by

Ravi Balgobin

Graduate Program in Chemical and Biochemical Engineering

A thesis submitted in partial fulfillment
of the requirements for the degree of
Master of Engineering Science

The School of Graduate and Postdoctoral Studies
The University of Western Ontario
London, Ontario, Canada

THE UNIVERSITY OF WESTERN ONTARIO
School of Graduate and Postdoctoral Studies

CERTIFICATE OF EXAMINATION

Supervisor

Dr. Dimitre Karamanev

Co-Supervisor

Dr. Amarjeet Bassi

Examiners

Dr. Madhumita Ray

Dr. Lars Rehmann

Dr. Julie Shang

The thesis by

Ravi Balgobin

entitled:

Bubble-free oxygen and carbon dioxide mass transfer in bioreactors using microporous membranes

is accepted in partial fulfillment of the
requirements for the degree of
Master of Engineering Science

Date

Chair of the Thesis Examination Board

Abstract

Increasing gas-liquid mass transfer in bioreactors is a major goal for performance improvement in bioprocesses. The effects of bubble-free oxygen and carbon dioxide mass transfer using microporous membranes were tested in a flat module and a hollow fiber module for applications in a bio-fuel cell and cultivation of microalgae. The volumetric mass transfer coefficient, $K_L a$, was compared to conventional bubbling. Liquid agitation rates influenced the mass transfer, as the limiting factor was the liquid boundary layer thickness. The $K_L a$ increased as the membrane hydrophobicity increased. The effect of pore size was found to be negligible for the hydrophobic membranes studied. The $K_L a$ for bubble-free aeration was found to be 2-3 times greater than bubbling at reduced power input. The growth rates of *Chlorella vulgaris* were found to be approximately 1.4 times higher than bubbling when utilizing bubble-free aeration in a hollow fiber module and in a novel flat membrane module.

Keywords

Renewable energy, bubble-free oxygen mass transfer, bubble-free carbon dioxide mass transfer, hydrophobic microporous membranes, bioreactor design, hollow-fiber module.

Co-Authorship Statement

Chapter 1- Introduction, Chapter 2- Literature review, Chapter 3- Flat membrane module- Oxygen mass transfer

R. Balgobin was the principal author. Revisions and recommendations were made by the supervisor Dr. D. Karamanev. A portion of Chapters 1, 2 and 3 was submitted for publication to the journal, *Chemical Engineering Science*, date of submission: March 20th, 2012.

Chapter 7- Cultivation of microalgae: bubbling versus bubble-free

R. Balgobin was the principal author. Revisions and recommendations were made by the supervisors Dr. D. Karamanev and Dr. A. Bassi. A portion of Chapter 7 will be prepared for a patent application.

Acknowledgments

I would like to sincerely thank my main supervisor, Dr. Dimitre Karamanev, for introducing me to his fascinating research on the Biogenerator and presenting me with the opportunity to work on this project. His support, guidance and all of his creative ideas are greatly appreciated. He will forever be a role model for many young students and researchers in this field. Many thanks are also given to my co-supervisor, Dr. Amarjeet Bassi, for his support and guidance and for giving me the opportunity to work on his captivating microalgae research. His innovative ideas are greatly appreciated. I would also like to thank Dr. Wankei Wan for motivation. A special thanks to my lab colleagues Mr. Victor Pupkevich, Dr. Kalin Penev and Dr. Jaydevsinh Gohil for all their assistance throughout this project. I would like to thank Mr. Brian Dennis and Mr. Souheil Afara for their assistance. Thanks to Ms. Ana Maria Aguirre for microalgae samples and media. Many thanks to Ms. Stephanie Drake and Dr. Denis O'Carroll for assistance with obtaining contact angles and use of their goniometer. I would also like to thank Ms. Jenna Allan and Dr. Paul Charpentier for assistance and use of their AFM machine.

Table of Contents

List of Tables

List of Figures

Chapter 1 : Introduction

In most bioreactors it is necessary to transport oxygen from gas to liquid as oxygen is the most important electron acceptor in bioprocesses (Garcia-Ochoa and Gomez, 2009; Garcia-Ochoa et al., 2010). Industrial microbial processes are mostly aerobic and the transfer of oxygen is usually the rate limiting step because of the low oxygen solubility in the media (Garcia-Ochoa and Gomez, 2009; Sadoff et al., 1956). The oxygen transfer rate greatly affects the cost, performance and the optimization of many bioreactors. Carbon dioxide mass transfer is also of importance as many microorganisms use it as their carbon source to facilitate growth for production of bio-fuels and other high valuable products (Carvalho and Malcata, 2001). Carbon dioxide is also one of the major greenhouse gases, and thus it is imperative to develop bioprocesses that can efficiently mitigate carbon dioxide emissions. It is therefore of great importance to improve and discover more efficient ways of gas transfer in bioprocesses.

1.1 Types of oxygen mass transfer

The following section describes methods of oxygen mass transfer to liquids and similar methods can be applied for carbon dioxide mass transfer to liquids.

There are several known ways of oxygen transfer to liquid media, the most popular being bubbling. By bubbling air or oxygen in the liquid media, it is possible to transport oxygen from the gas bubble through the gas film, through the gas-liquid interface, through the liquid film and then through the bulk of the liquid (Garcia-Ochoa et al., 2010). Oxygen transfer is subject to resistances through each step with the greatest resistance for mass

transfer being in the liquid film surrounding the bubble. Bubbling however possesses many constraints as the oxygen transfer rate is dependent on the size of the bubbles. The larger the bubbles supplied, the less surface area exposed for mass transfer of oxygen and a lower oxygen transfer rate will result. This is due to the proportionality between the oxygen transfer rate and the volumetric mass transfer coefficient, $K_L a$, where K_L is the mass transfer coefficient of the liquid side and a, is the total specific interfacial area available for mass transfer (Garcia-Ochoa and Gomez, 2009). If K_L or a is increased, greater oxygen mass transfer rates can be achieved. By breaking larger bubbles into smaller ones, the interfacial area can be increased, as there is a greater exposed bubble surface area and thus an increase in the oxygen transfer rate. This can be achieved by increasing the agitation rate in the bioreactor, however, high agitation speeds and high gas flowrates are energy intensive and also promote vigorous mixing which can damage any shear sensitive cells in the system and decrease the performance of the bioreactor.

Rotating biological contactors (RBC), and trickling filters are liquid film methods for oxygen mass transfer to liquid media. The both rely on the use of solid media to facilitate the gas-liquid contact. The rotating action of the RBC facilitates the oxygen transfer of the system as the liquid film is on moving solid media and is periodically exposed to the air. The oxygen transfer rate in an RBC is dependent on the exposed surface area and the contact time with the air (Patwardhan, 2003). In trickling filters, oxygen transfer is facilitated by contact of the upward flowing air with the liquid film flowing downward over the surface of static solid media. The large gas-liquid interfacial area makes it an attractive process for high oxygen transfer rates (Vasel and Schrobiltgen, 1991; Wilk, 2003).

Oxygen mass transfer can also be achieved by spraying liquid droplets in air using spray contactors. Oxygen diffuses from the air into the liquid droplets with the rate of oxygen transfer dependent upon the droplet size, column depth, recirculation rate, temperature and humidity (Chern and Yang, 2004; Kies et al., 2004). Electrolysis of the liquid media can also be employed to provide oxygen transfer to liquid media. This method involves the electrolytic cleavage of water and produces fine bubbles by the condensation of molecules (Sadoff et al., 1956). Higher current densities results in greater saturation oxygen concentrations and higher oxygen transfer rates (Franz et al., 2002).

Membrane aeration has been found to be a very attractive method for oxygen mass transfer in bioreactors as it can provide higher oxygen mass transfer rates compared to conventional methods and reduce energy input into the system (Ahmed and Semmens, 1992; Ahmed et al., 2004; Brindle et al., 1999; Cote et al., 1988, 1989; Gillot et al., 2005; Kreulen et al., 1993; Semmens, 2008). There are essentially two types of membrane aerators; fine bubble and bubble-free membrane aerators. Fine bubble membrane aerators utilize fine pore diffusers and can usually take the shape of discs, domes, tubes, plates and hollow fibers. There are also several disadvantages associated with the use of fine bubble diffusers as they are vulnerable to biological or chemical fouling which can hinder the mass transfer performance and generate large head losses and therefore must be cleaned routinely. Fine bubble membrane aeration generate higher oxygen transfer efficiencies as compared to conventional bubbling aeration as the interfacial area is greatly increased as the bubble size becomes very small which would result in a greater oxygen transfer rate into the liquid media (Gillot et al., 2005; Matsuoka et al., 1992). In aeration, the oxygen transfer rate is increased if the bubble size is decreased and ultimately, if the liquid is

aerated and is bubble-free, oxygen can diffuse through the membrane material and dissolve directly into the liquid media at a high oxygen transfer rate (Brindle et al., 1999; Voss et al., 1999). Bubble-free aeration has the potential to increase gas mass transfer and the performance of bioreactors and will be discussed in Chapter 2, Section 2.5.

1.2 Bioprocesses used in this thesis

1.2.1 Microbial fuel cell, the Biogenerator

With growing concerns on renewable energy sources, much emphasis has been placed on the hydrogen economy. Fuel cells are electrochemical devices that continuously generate electricity from the reaction between a fuel, usually hydrogen, and an oxidant, usually air or oxygen (Winter, 2005). One of the major drawbacks of conventional fuel cells is that the oxygen reduction reaction at the cathode has very slow kinetics (Ralph and Hogarth, 2002). Reduction of activation energy by high temperatures (greater than 600^{o}C) or usage of noble and expensive catalysts such as platinum is needed which increases cost. Redox fuel cells can increase the rate of the cathodic reaction as other oxidants, such as ferric irons, can replace oxygen and have higher reduction rates (Karamanev et al., 2010). Microorganisms have found a role in the optimization of fuel cells as iron oxidizing organisms, such as *Leptospirillum ferriphilum* can be utilized (Karamanev et al., 2010). Microbial fuel cells have emerged, and are electrochemical devices that utilize living microorganisms to continuously produce electrical energy from chemical energy. The Biogenerator is essentially microbial fuel cell and continuously produces electricity from hydrogen fuel and atmospheric oxygen from a polymer electrolyte membrane fuel cell combined with a bioreactor. The Biogenerator has several advantages associated with its

use as a fuel cell such as reduced costs, as platinum does not have to be used as a catalyst, and its long term stability (Pupkevich, 2007). A simplified schematic is depicted in Figure 1.1.

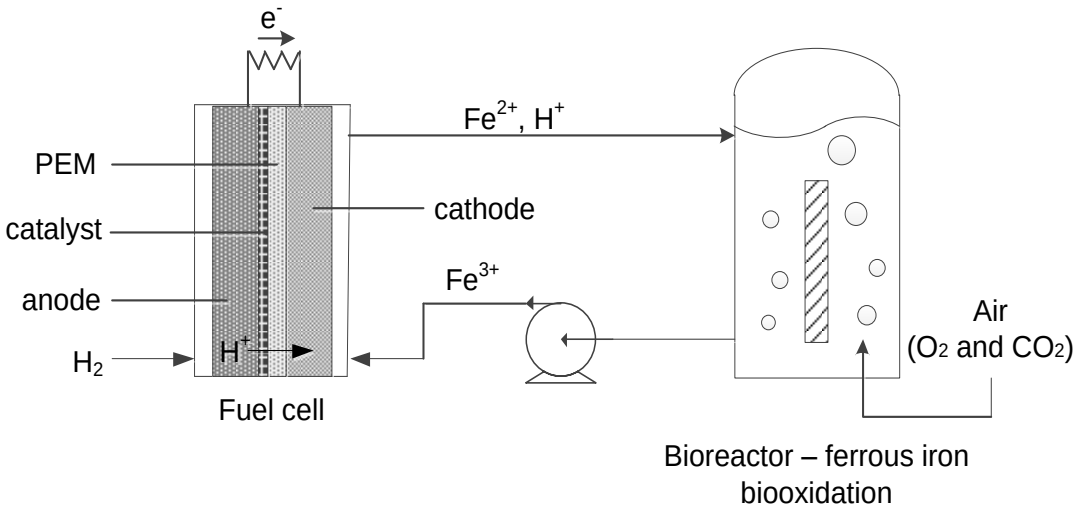

Figure 1.1. Schematic of the Biogenerator (Karamanev, 2009)

Hydrogen gas is indirectly oxidized in the fuel cell by the reduction of ferric iron to ferrous iron from the bioreactor solution according to the following (Karamanev, 2009):

$$4Fe^{3+} + 4e^{-} \rightarrow 4Fe^{2+} \quad (1.1)$$

Iron oxidizing microorganisms such as *L. ferriphilum*, regenerates the ferric iron by oxidizing the ferrous iron in the bioreactor according to the following (Karamanev, 2009):

$$4Fe^{2+} + 4H^{+} + O_2 \rightarrow 4Fe^{3+} + 2H_2O \quad (1.2)$$

The main bottleneck of this system and the limiting factor is the oxygen mass transfer rate in the bioreactor as it indirectly affects the overall performance due to the low solubility of oxygen in the media and the availability of oxygen to the microorganisms to facilitate ferrous iron oxidation. The oxygen is currently supplied by bubbling air, however, more efficient methods of oxygen mass transfer needs to be explored due to the inefficiencies of bubbling and significant operating costs associated with it. Bubble-free membrane aeration is a potential method of improving the oxygen mass transfer rate in this system and can also reduce aeration costs and thus will be analyzed in this project.

1.2.2 Cultivation of microalgae in photobioreactors

Microalgae have been used as far back as 2000 years ago by the Chinese, who used it as a food source to survive during times of famine (Spolaore et al., 2007). In the middle of the last century many applications of micro-algal biotechnology began to emerge. Because of the valuable products that can be extracted from micro-algal biomass, the product portfolio of micro-algal technologies are encompassed in the bio-fuel, water, nutraceutical, pharmaceutical and cosmetics industries (Harun et al., 2010). Due to their composition and fast growth rates, microalgae have found tremendous application worldwide. Within the past decade, microalgae have shown to have great potential in the production of bio-fuels and non-energy products. About 80 percent of the current global energy demand is produced from fossil fuels but the extensive use of fossil fuels have led to environmental pollution, health problems and global climate change (Chen et al., 2011). Some of the major issues with the usage of fossil fuels for energy production are the depleting supply of known reserves and the production of harmful greenhouse gases such as carbon dioxide. Due to these reasons there have been major incentives in the last

decade for industry leaders and researchers to design and implement renewable energy production methods which are necessary for environmental and economic stability (Chisti, 2007). Microalgae have the potential to produce bio-fuels and other high valuable products in a near carbon neutral process and mitigate carbon dioxide emissions as they require carbon dioxide as an energy source (Chen et al., 2011).

Microalgae are microscopic photosynthetic organisms that can be found in both freshwater and marine environments. They have a unicellular or simple multicellular structure which allows them to convert solar energy to chemical energy (Harun et al., 2010). Microalgae are photo-autotrophs that can be prokaryotic or eukaryotic. They are essentially sunlight-driven cell factories that can convert carbon dioxide to biomass. The main growth requirements are light, a carbon source such as carbon dioxide and nutrients such as nitrogen, phosphorous and other trace nutrients. During cultivation of microalgae in closed systems such as photobioreactors, the carbon dioxide mass transfer rate significantly affects the productivity and profitability. Carbon dioxide transfer to microalgal media is most conventionally done by bubbling air or a mixture of air and carbon dioxide. However, this is not the most efficient way of carbon dioxide mass transfer and a significant amount of carbon dioxide is then lost to the atmosphere which will add to operation costs (Carvalho and Malcata, 2001; Ferriera et al., 1998). With bubble-free carbon dioxide mass transfer, higher mass transfer rates can result which can increase productivity and reduce emissions, as it has the potential to recycle carbon dioxide (Carvallo and Malcata, 2001). Highly efficient membrane modules can also remove dissolved oxygen buildup that could inhibit micro-algal growth in closed photobioreactors (Cheng et al., 2006; Kumar et al., 2010).

1.3 Outlook of thesis

The main body of this thesis is separated into four parts. The first two chapters make up the introductory part of this work. In Chapter 1, an introduction into gas transfer in bioreactors and the importance of the gas mass transfer rate in bioreactors were discussed along with different methods of gas transfer. Two applications for this work were discussed; increasing oxygen mass transfer in a microbial fuel cell, the Biogenerator, and increasing carbon dioxide mass transfer for cultivation of microalgae in photobioreactors. The purpose of this research would conclude this chapter. Chapter 2 begins with an extensive literature review on membrane technology for bubble-free membrane gas mass transfer. A brief background on the history of membrane technology is presented followed by a description of the membrane parameters and characterization methods that are important for gas-liquid membrane contactors. The principles of gas transfer in bubbling and in bubble-free membrane aeration are discussed along with the significance of the volumetric mass transfer coefficient, $K_L a$, in comparing the gas transfer rates. Some general conclusions and reiteration of the main goals of this thesis are then presented at the end of Chapter 2.

The second part consists of experiments done with a flat flow-through membrane module to determine the effect of parameters such as liquid agitation speed, membrane hydrophobicity, membrane pore size, surface roughness and the effect of the membrane itself on the liquid mass transfer coefficient, K_L. Experiments done with air to determine relationships for oxygen mass transfer by bubble-free aeration are presented in Chapter 3. These include analyses done both with de-ionized water and with the bioreactor solution

from the Biogenerator. Major fundamental relationships will be concluded in this chapter. Experiments done with pure carbon dioxide to determine relationships for carbon dioxide mass transfer are presented in Chapter 4. The liquids used were both de-ionized water with a carbon dioxide buffer solution, and only the carbon dioxide buffer solution to maintain the pH of the liquid below 5 so that dissolved carbon dioxide can be measured efficiently.

The third part consists of bubble-free gas transfer experiments done with a hollow fiber membrane module that was selected based on the conclusion drawn form part 2. In Chapter 5, experiments are carried out with air to determine relationships for the volumetric mass transfer coefficient, K_La, of oxygen by bubble-free aeration and are compared to bubbling in the system. Both de-ionized water and the bioreactor solution from the Biogenerator are used as the liquid. The power input to the system is calculated and compared for bubbling and bubble-free aeration and the advantages of bubble-free aeration for increased oxygen mass transfer in the bioreactor solution are concluded. In Chapter 6 experiments were done with carbon dioxide and de-ionized water with the carbon dioxide buffer to analyze the bubble-free carbon dioxide mass transfer in the hollow fiber module and compare it to bubbling in the system.

The final part of this work presented in Chapter 7, is made up of experiments done to compare the growth rates of the micro-algal strain, *Chlorella vulgaris*, using bubble-free aeration and bubbling with atmospheric carbon dioxide. The growth rates of bubble-free aeration in a novel flat membrane photobioreactor and in a hollow fiber module are compared to bubbling under the same conditions. Finally the main conclusions and recommendations for future work are discussed in Chapter 8.

1.4 Purpose of this Research

Increasing the gas mass transfer rate in bioreactors is a crucial step in improving the overall performance of bioprocesses. Higher rates of oxygen dissolution will cause increased oxidation of ferric to ferrous iron by *L. ferriphilum* and result in greater performance of the Biogenerator. Increased carbon dioxide mass transfer also increases productivity for cultivation of microalgae in photobioreactors. Bubble-free membrane gas transfer is a potential method of increasing gas transfer and other studies on the membrane gas mass transfer have been primarily focused on hollow fiber modules. Unfortunately, due to the non-ideal fluid flow pattern, the conditions in such a design do not allow for the determination of the fundamental relationship between the membrane characteristics and the fluid parameters, at one side, and the gas mass transfer coefficient, at the other. In our view, the fundamental characteristics of the bubble-free membrane gas transfer can be determined most precisely using flat membrane geometry and then be applied to a hollow fiber module.

1.4.1 Main objectives

- To fundamentally determine the effects of membrane material, hydrophobicity, pore size and agitation speed on the bubble-free oxygen and carbon dioxide mass transfer using flat microporous membranes in a flow-through module.
- To determine the optimum membrane characteristics for bubble-free gas transfer to liquids using a hollow fiber module.

- To increase the volumetric mass transfer coefficient, for oxygen in de-ionized water and in the bioreactor solution of the Biogenerator, using a hollow fiber module and compare the mass transfer to bubbling under the same conditions.
- To increase the volumetric mass transfer coefficient, for carbon dioxide in de-ionized water with a carbon dioxide buffer solution, using a hollow fiber module and compare the mass transfer to bubbling under the same conditions.

1.4.2 Secondary objectives

- To compare the approximate power inputs from bubbling and bubble-free aeration and determine which method has more efficient oxygen mass transfer at reduced power input both in de-ionized water and in the Biogenerator media.
- To determine the growth rates of the micro-algal strain, *C. vulgaris*, using bubble-free aeration in a novel flat membrane photobioreactor and in a hollow fiber module, and compare them to bubbling under the same conditions.

Chapter 2 : Literature Review

2.1 Background on Membrane technology

The study of membranes can be dated back as far as the 18th century. In 1748, Abbe Nolet used the word "osmosis" to explain the permeation of water through a diaphragm (Baker, 2004). In 1887 van't Hoff developed his limit law and his equation from data of solution osmotic pressure from Pfeffer and Traube (Baker, 2004). Maxwell and others used the concept of a selective semipermeable membrane to develop the kinetic theory of gases. Membranes had found their first major application around the end of World War II in the testing of drinking water. From the 1960's through to the 1980's, membrane science and technology had made significant advancements. To date membranes have found applications in microfiltration, ultrafiltration, reverse osmosis, electrodialysis, membrane contactors, water purification, gas separations, tissue repair, fuel cells, pharmaceutical production, the food and beverage industry and the clothing industry (Li et al., 2008). Membranes have also found a wide array of application as membrane contactors where the membrane serves as an interface between two phases. Membrane contactors have the advantage of having higher surface areas to volume than other contactors such as packed columns, tray columns, free dispersion columns and mechanically agitated columns. Membrane contactors are easier to scale up and less energy intensive. The membrane can be used as a gas-liquid or a liquid-liquid contactor. Gas-liquid contactors are used to either add or remove dissolved gases to or from liquids (Baker, 2004). The characteristics and applications of various types of membranes are vast and as such, only those relating

to polymer membranes as gas-liquid contactors will be discussed here where gas flows on one side and liquid flows on the other of the membrane.

A membrane is essentially a thin, discrete film that can control the permeation of a chemical species that is in contact with it (Baker, 2004). Molecularly homogenous membranes are completely uniform in structure and composition. Physically or chemically heterogeneous membranes contain pores of finite size or a layered structure. Membranes can be further classified as natural or synthetic. Synthetic membranes can be divided into organic and inorganic, with the most important in this study being organic (polymeric). Membrane transport can be driven by differences in concentration, pressure, temperature or electrical potential. With relation to usage in gas-liquid contactors, polymeric membranes are divided into nonporous (dense) membranes, or porous membranes.

2.1.1 Nonporous membranes

Nonporous membranes are made up of a dense film where the permeants are transported by diffusion. The diffusivity and solubility of various components of a mixture in the membrane determines the relative transport rate within the membrane (Baker, 2004). Dense membranes have the ability to separate permeants of similar size if there are significant differences of the solubility in the membrane material. Gas Permeation through dense polymer membranes can be described by a Solution-diffusion model as shown in Figure 2.1.

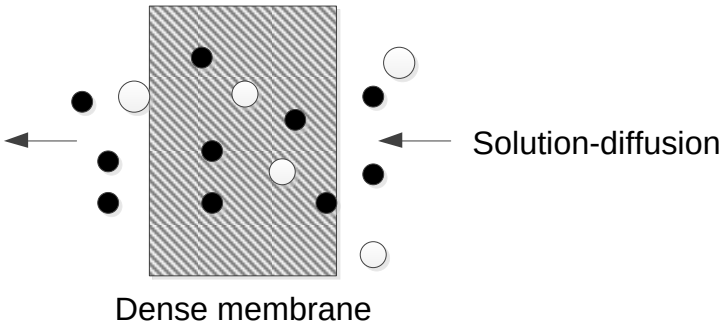

Figure 2.1. Solution diffusion model for dense membranes (Baker, 2004)

The solute dissolves in the membrane and diffusion takes place in the free volume between the membrane's macromolecular chains. The permeability of a gas molecule through the membrane is given by the following (Li et al., 2008):

$$P = D.\ S \qquad (2.1)$$

where P is the permeability coefficient; D is the diffusion coefficient; and S is the solubility coefficient. The oxygen permeability in various polymers is shown in Table 2.1. Silicone rubber is one of the most oxygen permeable materials. The diffusivity of most gases in a gas is significantly greater than the diffusivity of a gas in a liquid, and greater than the diffusivity of a gas in solids. This can be demonstrated by the diffusion coefficient of oxygen in various media as shown in Table 2.2.

Table 2.1. Permeability of oxygen in various polymers (Cote et al., 1989)

Polymer	Permeability* (cm3-cm/cm^2 cmHg) x l0^9
Dimethyl silicone rubber	60
Fluorosilicone	11
Nitrile silicone	8.5
Natural rubber	2.4
Polyethylene, low density	0.8
Polypropylene	0.2
BPA polycarbonate	0.16
Butyl rubber	0.14
Cellulose acetate	0.08
Poly(viny1 chloride)	0.014
Poly(viny1 alcohol)	0.01
Nylon 6	0.004
Poly (vinylidene fluoride)	0.003
PTFE	0.004

*Multiply values by 3.35 x 10^{-6} to obtain units in mol.m^{-1}.s^{-1}.Pa^{-1}

Table 2.2. Diffusion coefficients of oxygen in various media at 25^{o}C (Baker, 2004)

Permeant/ media	Diffusion Coefficient (cm^2.s^{-1})
Oxygen in air (atmospheric)	1 x 10 $^{-1}$
Oxygen in water	2 x 10 $^{-5}$
Oxygen in silicone rubber	1 x 10 $^{-5}$

2.1.2 Porous membranes

Porous membranes have highly voided and firm structures with interconnected pores that are randomly distributed. Particles which are much smaller than the smallest pore can pass through the membrane. The membrane completely rejects particles that are larger than the largest pores. Particles which are larger than the smallest pores but smaller than the largest pores are only partially rejected according to the membrane pore size distribution. The separation of solutes is primarily a function of pore size distribution and molecular size. Table 2.3 shows the sizes of common gases used in this study.

Table 2.3. Gas molecular sizes (Baker, 2004)

Gas	Kinetic diameter (Å)	Lennard Jones Diameter (Å)
Nitrogen	3.64	3.8
Oxygen	3.46	3.47
Carbon Dioxide	3.3	3.94

The Kinetic diameters are based on molecular sieve measurements whereas the Lennard Jones diameter is based on viscosity measurements.

The type of diffusion in porous membranes is based on differences in pore size. This is illustrated in Figure 2.2.

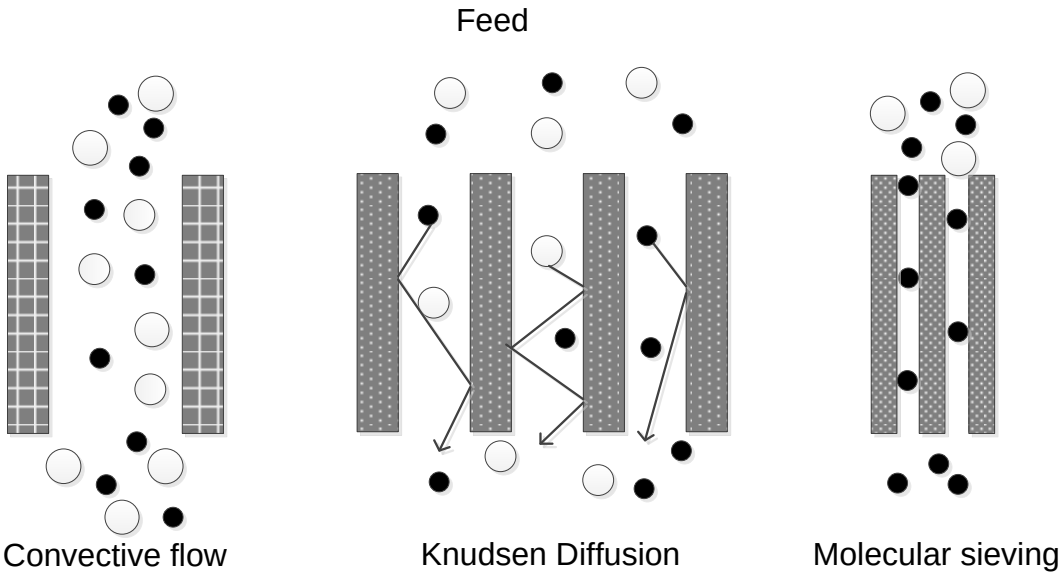

Figure 2.2. Types of diffusion in porous membranes (Baker, 2004)

Gases will permeate the membrane by convective flow and no separation will occur if the pore size is relatively large, around 0.1 to 10μm. Knudsen diffusion occurs if the pore size is less than 0.1μm. During Knudsen diffusion, the pore diameter is equal to or smaller than the mean free path of the molecules and according to Graham's law of diffusion, the transport rate of any gas is inversely proportional to the square root of its molecular weight. The gas molecules will collide more with the pore of the walls than other gas molecules as the ratio of the pore radius to the gas free mean path is below 1 for Knudsen diffusion. Gases are separated by molecular sieving if the pore size of the membranes is very small and around 5 Å to 20Å. This type of transport is complex and combines gaseous diffusion with surface diffusion, which is diffusion of the adsorbed species on the pore surface (Baker, 2004).

The membrane pore size determines the particle diameter that it can retain with a high degree of efficiency. It can be measured by using a challenge organism, bubble point analysis or porosimetry. The nominal pore size gives the pore size that the filter will retain the majority of the particle at about 60-98% efficiency. The absolute pore size is the pores size that a challenge organism will be retained at approximately 100% efficiency at strictly defined conditions. According to the IUPAC, the pores in membranes are also classified based on their pore sizes with macropores being larger than 50nm; mesopores between 2 to 50nm; and micropores being smaller than 2nm (IUPAC, 1985). However, many authors have reported usage of microporous membranes with pore sizes between 0.01 to 0.45μm (Ahmed and Semmens, 1992; Baker, 2004; Carvalho et al., 2001; Ferrera et al., 1998; Kreulen et al., 1993) and as a result we classified our membranes used in this project as microporous.

The membrane porosity or the void volume is equal to the pore volume divided by the volume of the membrane material. Research into carbon dioxide mass transfer in a membrane gas-liquid contactor has shown that at pH less than 11, increasing the average membrane porosity did not have a significant effect on the volumetric mass transfer coefficient (Zhang et al., 2010).

2.1.3 Hydrophobicity

Membranes have either hydrophilic or hydrophobic properties based on the material's chemical characteristics. Hydrophilic membranes possess an affinity to water and are wetted easily. Wetting favors membranes with high surface energies. When wetting occurs, water penetrates the pores of the membrane. Liquids with higher surface tensions,

like water, can more easily wet a hydrophilic membrane than a liquid with low surface tension. Hydrophobic membranes lack an affinity towards water and are not easily wetted. Membrane hydrophobicity is measured by the contact angle. The contact angle is measured with a goniometer and measures the angle of a droplet of water on the membrane surface. Hydrophilic membranes form contact angles from 0 to 90^o and hydrophobic membranes form contact angles contact angles from 90^o to150^o. This effect is illustrated in Figure 2.3.

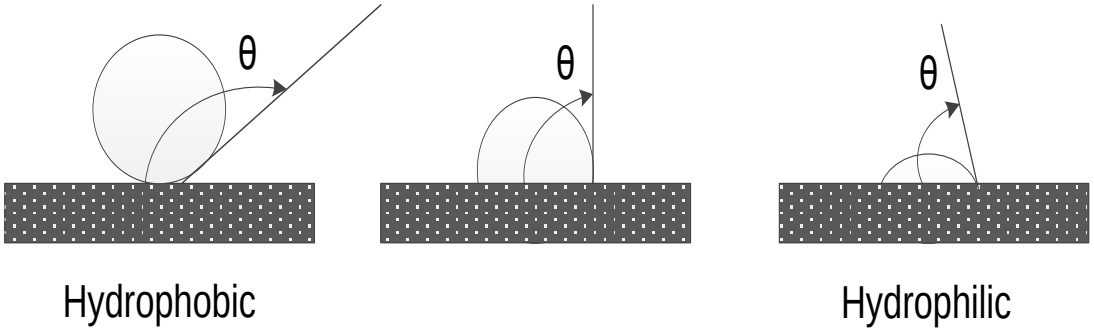

Figure 2.3. Measurements of membrane contact angle

Superhydrophobic membranes have contact angles between 150^o to180^o (Xue et al., 2010). Hydrophobic porous membranes do not allow liquids to enter their pores unless the pressure difference between the liquid and gas streams is greater than the breakthrough pressure (Lv et al., 2011). This is given by the following:

$$\Delta P = -\frac{4\sigma_L cos\theta}{d_P} \tag{2.2}$$

where ΔP is the penetration pressure difference; σ_L is the surface tension of the liquid; θ is the contact angle between the membrane and the liquid phase; and d_P is the pore size, m.

2.1.4 Membrane geometry and modules

Depending on the application, membranes can have a wide range of geometries. They can be either flat or cylindrical. Flat membranes are essentially thin flat sheets or disc filters and are widely used for general filtration purposes based on their pore sizes and material of construction. Modules made from flat membranes include plate and frame, and spiral wound membranes (Baker, 2004). The plate and frame module consist of the membrane, feed spacers and product spacers that are stacked together between two end plates. Spiral wound modules consist of a membrane envelope that is wrapped around a collection tube.

Cylindrical modules are classified based on their dimensions and can be either tubular or hollow fiber in configuration. Tubular membranes have diameters approximately greater than 5mm and the tubes are made of a porous fiberglass or paper support with the membrane casted on the inside. Hollow fiber membranes have internal diameters approximately less than 5mm. Hollow fiber membrane modules have the advantage over other configurations of having very large surface area to volume ratios as thousands of hollow fibers can be packed into a small module. Hollow fibers can have open ended tubes or sealed ended tubes.

2.1.5 Types of flow in membranes

The flow through membranes can be either dead end or cross (tangential) flow. In dead end flow, the feed stream is perpendicular to the membrane. This is illustrated in Figure 2.4.

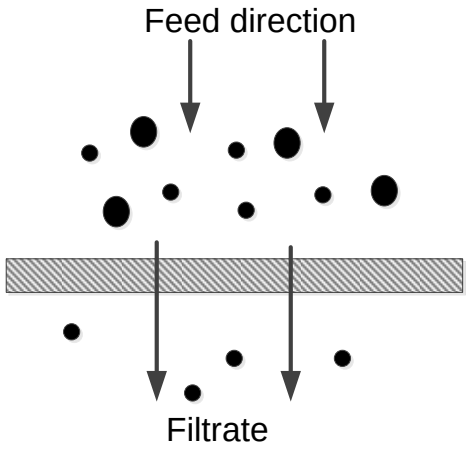

Figure 2.4. Dead end filtration

This configuration has the disadvantage of increasing pressure and reducing flow over time as particles and aggregates can build up. In tangential flow, the feed stream moves parallel to the membrane surface. Unlike dead end filtration, tangential flow continuously sweeps the surface of the membrane as the feed stream circulates across it which results in minimal blockage of membrane pores and greater long term productivity. This is illustrated in Figure 2.5.

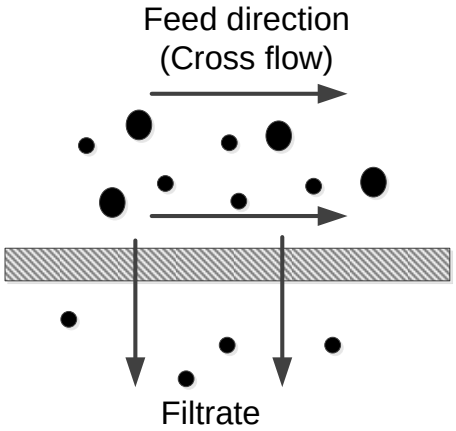

Figure 2.5. Tangential flow filtration

In gas-liquid membrane contactors, the flow of the two streams can be either co-current or counter current. In co-current flow the gas and liquid streams flow parallel and in the same direction. This situation is avoided for gas transfer as the flux through the membrane is decreased due to lower concentration gradients. In counter current flow, the gas and liquid streams flow in opposite directions and results in a more controlled and larger concentration gradient with improved flux and performance (Baker, 2004).

2.2 Gas mass transfer by bubbling

During bubbling in bioprocesses, the gas is transferred from the rising gas bubble and dissolved into the liquid media and then ultimately transported to the cell. This involves a number of steps the resistances for the gas to reach the microbial cell include (Garcia-Ochoa and Gomez, 2009):

- the bulk gas phase from inside bubble
- the gas-liquid interface
- the liquid film surrounding the bubble
- the bulk liquid
- the liquid film around the microbial cell
- the intracellular gas transfer resistance

The gas-liquid mass transfer can be modeled according to the two film theory which states that all the mass transfer resistance occurs in a thin film on each side of the gas-liquid interface. This is depicted in Figure 2.6.

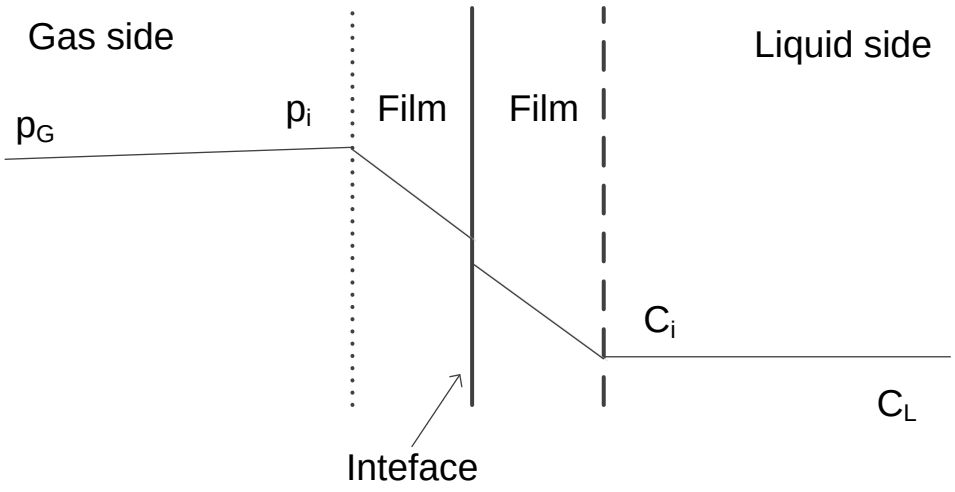

Figure 2.6. Mass transfer model for bubbling

The flux through each film is given is given by:

$$J = k_G H (p_G - p_i) = k_L (C_i - C_L) \quad (2.3)$$

where J is the molar gas flux through the gas-liquid interface; p_G is the gas partial pressure in the bubble; p_i is the interface gas partial pressure; k_G and k_L are the local mass transfer coefficients in the gas and liquid phases; H is the Henry's constant; C_L is the dissolved gas concentration in the bulk liquid; and C_i is the interface liquid concentration.

Assuming that the concentration of the gas on the interface is saturated, the following equation results:

$$J = K_G H (p_G - p^*) = K_L (C^* - C_L) \quad (2.4)$$

where p^* is the gas pressure in equilibrium with the liquid, K_G and K_L are overall mass transfer coefficients of the gas and liquid phases; C^* is the saturation gas concentration in

the bulk liquid in equilibrium with the gas phase and is given according to Henry's law ($p^* = HC^*$).

If Equations (2.3) and (2.4) are combined, the following relationship results:

$$\frac{1}{K_L} = \frac{1}{k_L} + \frac{1}{Hk_G} \tag{2.5}$$

Since H is large for gases such as oxygen that is only slightly soluble in water, the gas phase coefficient can usually be considered negligible and the greatest resistance to mass transfer will lie in the liquid phase and thus $K_L = k_L$.

If the overall flux is multiplied by the specific interfacial area, a, the following relationship is obtained:

$$N_{gas} = J.a = K_L a\ (C^* - C_L) \tag{2.6}$$

where N_{gas} is the gas mass transfer rate per unit volume of reactor; and $K_L a$ is the volumetric mass transfer coefficient, which is a measure of the transport form gas to liquid. During bubbling, K_L and a are difficult to measure separately and thus the volumetric mass transfer coefficient, $K_L a$, is usually measured. Therefore, increasing the $K_L a$ of a system increases the gas transfer rate.

2.3 Gas transfer in gas-liquid membrane contactors

Analogous to bubbling, the gas mass transfer to liquid media through gas-liquid membrane contactors is subjected to a series of steps and resistances which will vary based on the type of membrane used (Aptel and Semmens, 1996):

- The bulk gas through the gas film on the membrane

- The gas membrane interface
- Through the membrane (and the pores for porous membranes)
- The membrane liquid interface
- The liquid film on the membrane
- The bulk liquid

A resistance in series model is used to describe the gas mass transfer through membranes and chemical transfer occurs by molecular diffusion through the stagnant film on each side of the membrane and the membrane itself (Aptel and Semmens, 1996). This is illustrated in Figure 2.7.

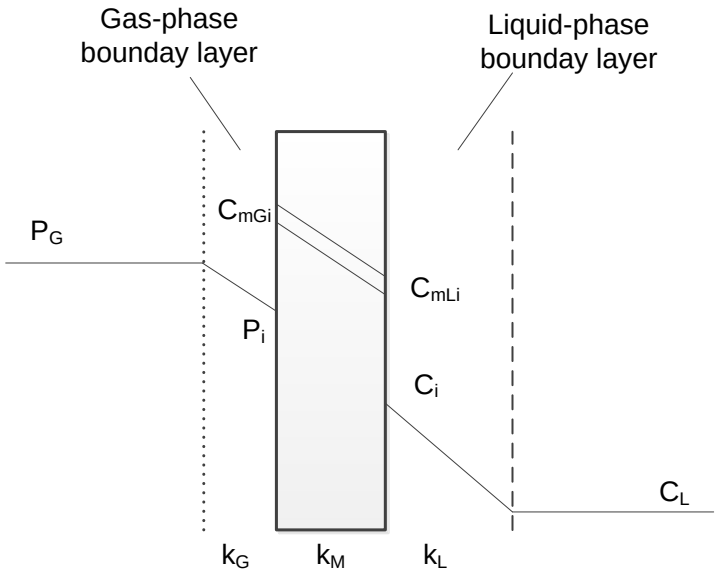

Figure 2.7. Resistances to membrane gas transfer (Aptel and Semmens, 1996)

The flux through each film is given by:

$$J = k_G H(p_G - p_i) = k_M K_D (Cm_{Gi} - Cm_{Li}) = k_L (C_i - C_L) \quad (2.7)$$

where Cm_{Gi} and Cm_{Li} are the membrane interface gas and liquid concentrations, k_M is the membrane mass transfer coefficient; K_D is the dimensionless equilibrium partition coefficient; H is the dimensionless Henry's law constant given by the ratio of the concentrations of the gas and liquid phases at equilibrium.

Similar to bubbling, the interfacial concentrations are difficult to measure and the flux can be expressed in terms of the bulk concentrations and ultimately lead to Equations (2.4) and (2.6). Thus the volumetric mass transfer coefficient K_La, can be determined and used as an indication of the gas transfer rate to the liquid. The overall liquid mass transfer coefficient K_L, will depend on the type of membrane used (Aptel and Semmens, 1996).

For dense membranes the overall liquid mass transfer coefficient is given by:

$$\frac{1}{K_L} = \frac{1}{k_L} + \frac{1}{K_D k_m} + \frac{1}{H k_G} \tag{2.8}$$

For porous membranes, if liquid fills the pores in hydrophilic membranes, the overall liquid mass transfer coefficient for is given by:

$$\frac{1}{K_L} = \frac{1}{k_L} + \frac{1}{k_m} + \frac{1}{H k_G} \tag{2.9}$$

For porous membranes, if the pores are filled with gas in hydrophobic membranes, the overall liquid mass transfer coefficient is given by:

$$\frac{1}{K_L} = \frac{1}{k_L} + \frac{1}{H k_m} + \frac{1}{H k_G} \tag{2.10}$$

When gas occupies the pores, $1/K_L \approx 1/k_L$, as H is high for sparingly soluble gases in water like oxygen and more soluble gases like carbon dioxide.

2.4 Determination of the volumetric mass transfer coefficient, K_La

It is essential to determine the volumetric mass transfer coefficient in bioreactors so that aeration efficiencies and the effects of operating conditions on the dissolved gas concentration can be determined. In the case of dissolved oxygen, the mass balance in a well mixed liquid is given by (Garcia-Ochoa and Gomez, 2009):

$$\frac{dC}{dt} = OTR - OUR \tag{2.11}$$

where dC/dt is the accumulation rate of oxygen in the liquid, OTR is the oxygen transfer rate given by Equation (2.6) and OUR is the oxygen uptake rate by the microorganisms which is equal to $q_{O2}.C_X$, where q_{O2} is the specific oxygen uptake rate of the microorganisms and C_X is the biomass concentration. If no microorganisms are present in the media, the OUR = 0 and results in the following (Garcia-Ochoa and Gomez, 2009):

$$\frac{dC}{dt} = K_La\,(C^* - C) \tag{2.12}$$

A similar analysis can be done for carbon dioxide however since carbon dioxide is an acid gas that reacts with water, the values of K_La are pH dependent and can be adjusted to any pH which will be shown later.

The K_La can be determined by physical, biological and chemical methods. Physical methods are based on measurements of the changes in dissolved gas concentration over

time with the use of dissolved gas probes. Chemical methods of K_La determination involve the addition of chemicals and result in changes in fluid dynamics and more variability in the results as chemical reactions can enhance the transfer rate (Garcia-Ochoa and Gomez, 2009). Therefore, physical methods are preferred with the dynamic method, which involves the absorption and desorption of the dissolved gas, being the most commonly used due to its relative accuracy and ease of estimation. This will be discussed later.

2.5 Bubble-free membrane gas transfer

Bubble-free gas transfer is achieved by diffusing gas through gas permeable dense or microporous membranes to liquid media without the formation of bubbles (Ahmed and Semmens, 1992; Cote et al., 1988, 1989). In dense polymer membranes, the gas is absorbed on the gas side of the membrane and diffuses through the membrane and into the liquid (Cote et al., 1988, 1989). The most oxygen permeable dense polymer membranes are made of silicone rubber and can be operated at high gas pressures without bubble formation (Cote et al., 1988). However, silicone membranes are more expensive, thicker and exhibit a higher mass transfer resistance than microporous membranes (Ahmed and Semmens, 1992). Recent researchers have found that the oxygen mass transfer coefficients for microporous polypropylene were approximately three times higher than that of dense silicone (Duan et. al, 2010). Due to these reasons, microporous membranes will be tested in this study. In microporous membranes, the pores are filled with either gas (in the case of hydrophobic membranes) or with liquid (in hydrophilic membranes) (Cote et al., 1988, 1989). Instead of diffusion through the polymer, the gas is

diffused through the gas or liquid filling the pore system in microporous membranes due to the concentration gradient. This is depicted in Figure 2.8.

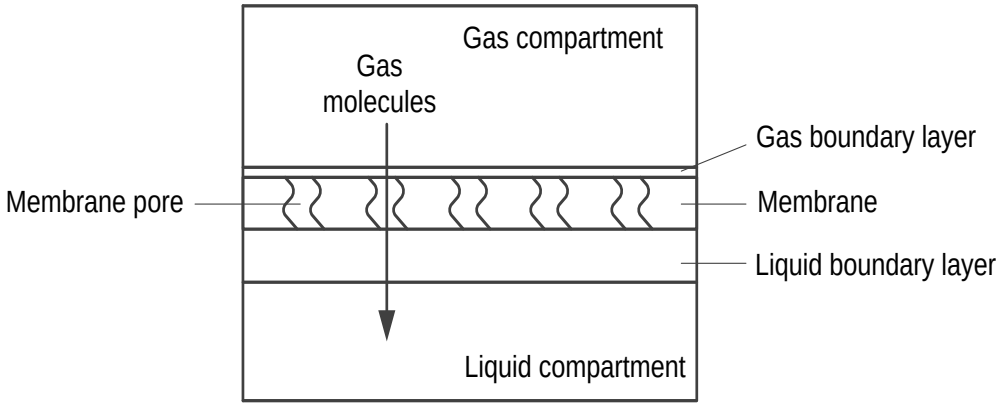

Figure 2.8. Bubble-free membrane gas mass transfer

The reverse can be done with nitrogen as a sweep gas for the desorption of dissolved oxygen. The dissolved oxygen concentration in the liquid is small but its equilibrium concentration in the gas phase that is in contact with the liquid is significantly larger and thus a high permeation rate down the concentration gradient to the nitrogen sweep results (Baker, 2004). Oxygen is desorbed from the liquid, moves through the membrane pores and is then swept away by nitrogen. This is illustrated in Figure 2.9.

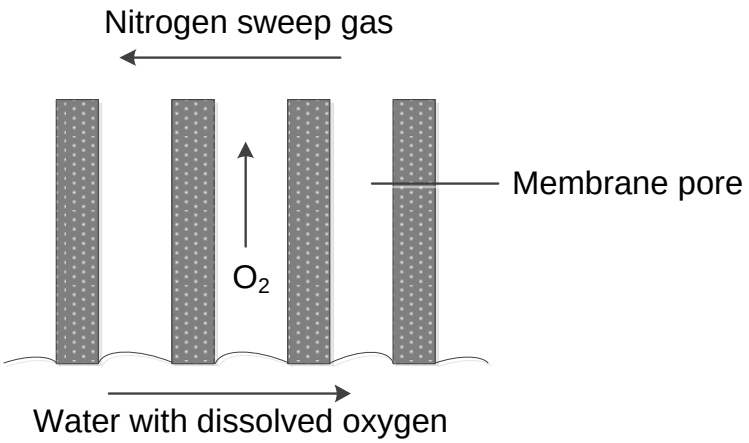

Figure 2.9. Bubble-free membrane desorption of oxygen (Baker, 2004)

The pressure difference between the gas and liquid side should not exceed the bubble point of the microporous membrane for bubble-free aeration to occur. If the liquid side is pressurized then a high gas pressure can be utilized (Cote et al., 1988). Bubble-free membrane aeration has several advantages over conventional methods which include (Ahmed and Semmens, 1992; Semmens, 2008):

- higher mass transfer rates due to higher interfacial areas that can be achieved
- less energy input as aeration costs are reduced as no hydrostatic head as in bubbling
- lower shear stress compared to bubbling
- no volatilization of volatile organic compounds

Some potential disadvantages include biofilm formation that can reduce the performance of the membrane, and the cost which depends on the membrane material used.

Recent research has been focused almost exclusively on the use of the hollow fiber configuration in microporous membranes for bubble-free aeration (Ahmed et al., 2004;

Duan et al., 2010; Semmens, 2008). There are two main types of gas flow for bubble-free gas transfer in hollow fiber configurations; sealed end and flow through. In sealed end hollow fibers, all the gas is forced through the wall of the membrane and 100% gas transfer efficiency can be achieved. A potential decrease in performance is more likely to occur over time in sealed end hollow fibers as a back-flux of nitrogen and carbon dioxide could occur if air is used and water may condense in the fibers if there is a temperature drop (Ahmed et al., 2004; Cote et al., 1988; Semmens, 2008). If pure oxygen or carbon dioxide is the gas being used for aeration then a sealed ended configuration would be advantageous. If air is being used, then a flow through configuration would be preferred.

2.6 Conclusions from literature review

The use of membranes as gas liquid contactors as an alternative to bubbling is a potential way of increasing gas mass transfer in bioreactors due to the higher interfacial areas that can be achieved. Microporous membranes operating in a flow through configuration have been shown to have better gas mass transfer rates than dense membranes in a sealed end configuration when air is used. As shown above, there are many studies on the gas mass transfer using hollow fiber membranes. However, due to the non-ideal fluid flow pattern, the conditions in such a design do not allow to determine the fundamental relationship between the membrane characteristics and the fluid parameters, at one side, and the oxygen and carbon dioxide mass transfer coefficient, at the other. In our view, the fundamental characteristics of the bubble-free membrane gas transfer can be determined most precisely using a flat membrane geometry. The main goals of this work are therefore to fundamentally determine the effects of membrane

material, hydrophobicity, pore size and agitation speed on bubble-free aeration of water using flat microporous membranes in a flow-through module and to apply these findings for usage in a hollow fiber module for oxygen mass transfer and carbon dioxide mass transfer to liquids.

2.7 Nomenclature

C*	saturation gas concentration in the bulk liquid	$mol.L^{-1}$
K_La	volumetric mass transfer coefficient	s^{-1}
C_i	interface liquid concentration	$mol.L^{-1}$
C_L	dissolved gas concentration in the bulk liquid	$mol.L^{-1}$
Cm_{Gi}	membrane interface gas concentration	$mol.L^{-1}$
Cm_{Li}	membrane interface liquid concentration	$mol.L^{-1}$
D	diffusion coefficient	$cm^2.s^{-1}$
d_P	pore size	m
H	dimensionless Henry's law constant	-
J	molar gas flux	$mol.m^2.s^{-1}$
K_D	dimensionless equilibrium partition coefficient	-
k_G	local mass transfer coefficient in gas phase	$m.s^{-1}$
k_L	local mass transfer coefficient in liquid phase	$m.s^{-1}$
K_G	overall mass transfer coefficient in gas phase	$m.s^{-1}$
K_L	overall mass transfer coefficient in liquid phase	$m.s^{-1}$

K_La	volumetric mass transfer coefficient	s^{-1}
k_M	membrane mass transfer coefficient	$m.s^{-1}$
N_{gas}	gas mass transfer rate per reactor volume	$mol.s^{-1}.L^{-1}$
P	permeability coefficient	cm^3 stp cm/ cm^2 s cm Hg
ΔP	penetration pressure difference	kPa
p^*	gas pressure in equilibrium with the liquid	Pa
p_G	gas partial pressure	Pa
p_i	interface gas partial pressure	Pa
S	solubility coefficient	cm^3gas/ cm^3polymer cm Hg

Greek letters:

σ_L	surface tension of the liquid	$mN.m^{-1}$
θ	contact angle	degrees

Chapter 3 : Flat membrane module- Oxygen mass transfer

A flat membrane module acting as a gas-liquid contactor was constructed and used to fundamentally determine the effects of agitation, membrane material, hydrophobicity, pore size and the effect of the membrane itself on the oxygen mass transfer in bubble-free aeration of both de-ionized water in Sections 3.1 and 3.2, and a bioreactor solution from the Biogenerator in Section 3.3.

3.1 Materials and Methods

3.1.1 Membranes and parameters

The flat sheet membranes used in this study were Polypropylene (Sterlitech, Kent, WA, USA), PTFE (Sterlitech), Polycarbonate (Sterlitech), Nylon-6,6 (Pall Co., Port Washington, NY, USA), Polyethersulfone (Pall Co.) and Hydrophilic Polypropylene (Pall Co.). The properties of the membranes are summarized in Table 3.1. The contact angles of the 0.22μm hydrophobic membranes were obtained using an Axisymmetric Drop Shape Analyzer, FTA 1000 C Class (First Ten Angstroms, Portsmouth, VA, USA). Static contact angles were measured as it was done for a general comparison basis. A 1μL drop of de-ionized water was used on 5 different locations on the membrane surface, to reduce the error in measurement, and the results were averaged.

Table 3.1. Membrane parameters

Material	Type	Pore size, µm	Thickness, µm	Porosity, %
Polypropylene	Hydrophobic	0.10	92.5	63
Polypropylene	Hydrophobic	0.22	150	67
Polypropylene	Hydrophobic	0.45	155	74
PTFE	Hydrophobic	0.22	71.0	70
Polycarbonate	Hydrophobic	0.22	10.0	9.4
Polycarbonate	Hydrophobic	0.45	10.0	13
Polypropylene	Hydrophilic	0.45	114	72
Polyethersulfone	Hydrophilic	0.10	129	69
Polyethersulfone	Hydrophilic	0.45	114	73
Nylon-6,6	Hydrophilic	0.45	158	75

The surface roughness of the 0.22µm hydrophobic membranes was measured using an Atomic Force Microscope (Veeco, Plainvew, NY, USA) in tapping mode in a 7µm x 7µm area and analyzed with Nanoscope 7.0 software (Veeco). The Root Mean Square (RMS) roughness value was obtained after flattening the image.

3.1.2 Experimental setup

The experimental configuration used in this study is depicted in Figure 3.1.

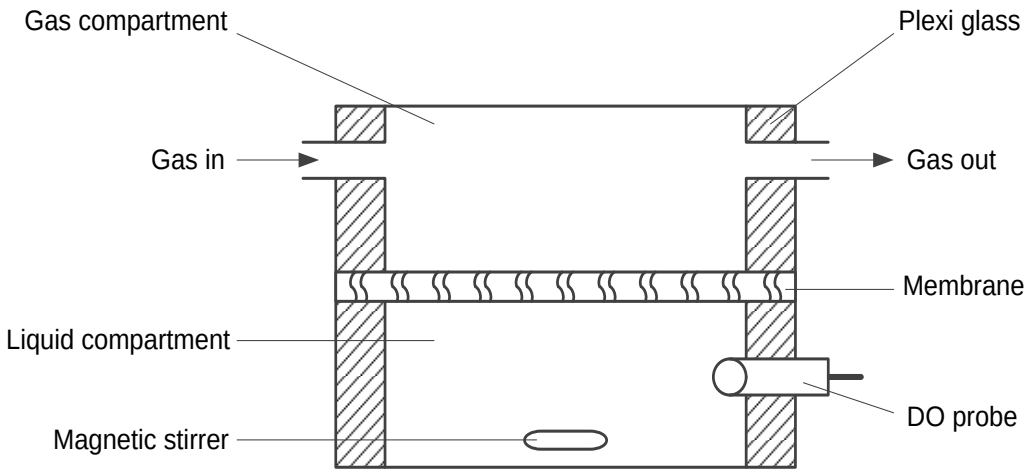

Figure 3.1. Schematic of experimental setup for oxygen mass transfer in the flat module

The exposed geometrical surface area of the membranes was 8.04cm^2. The volumes of the liquid and gas compartments were 12.1cm^3 each. De-ionized water was used as the liquid medium and a 0.5 inch magnetic stir bar (VWR) was used for agitation in the liquid compartment. Air was supplied to the gas compartment at a flowrate of 100L.h^{-1} using a Rena Air 400 pump (Rena, Chalfont, PA, USA). Nitrogen (95%), (Praxair Canada, Mississauga, Ontario, Canada) was alternately supplied at the same flowrate as air. The flow-through module maintained the gas pressure at near atmospheric and below the bubble point of the membranes. The dissolved oxygen (DO) concentration in liquid was measured with an Orion 081010MD polarographic dissolved oxygen probe (Thermo Scientific, Nepean, Ottawa, Canada) connected to an Orion 3 star meter (Thermo Scientific). The probe was calibrated by saturating de-ionized water with air. A zero point calibration was also done by sparging de-ionized water with nitrogen. The liquid temperature was maintained at 24^{o}C.

3.1.3 Determination of the DO probe lag and the response time

Two 100mL beakers were filled with de-ionized water with beaker 1 being saturated with air and beaker 2 being sparged with nitrogen to achieve a near zero dissolved oxygen concentration. The probe was placed in beaker 1 and allowed to equilibrate. After equilibration, the probe was subjected to a nearly instantaneous change in dissolved oxygen concentration by being placed in beaker 2. The dissolved oxygen concentration was recorded over time. The probe lag was modeled as a first-order differential equation according to the following (Philichi and Stenstrom, 1989):

$$\frac{dC_p}{dt} = \frac{C - C_p}{\tau} \tag{3.1}$$

where C_p is the DO indicated by the probe at time, t; C is the actual DO; and τ is the probe lag constant. After integration and linearization, the above equation becomes:

$$ln\frac{C - C_p}{C - C_{po}} = \frac{-t}{\tau} \tag{3.2}$$

where C_{po} is the initial probe reading. The probe lag constant was estimated by plotting the above equation. The response time of the probe was determined as the percentage of the steady state value achieved over a period of time when the probe was subject to an instantaneous change in DO concentration by switching from beaker 1 to beaker 2. Three trials were done and the mean value was used.

3.1.4 Determination of K_L

The dynamic method was used in this study to determine the overall liquid mass transfer coefficient, K_L, of each membrane studied. De-ionized water was deoxygenated to a near zero concentration by sparging with nitrogen and then transferred to the liquid compartment of the cell. The air flow was turned on at 100L.h^{-1} and the DO concentration monitored over time at a set liquid stirrer speed. After reaching near steady state, the air was turned off and the nitrogen flow was turned on at 100L.h^{-1}. For each trial, the air on/air off cycle was performed twice to generate 4 cycles for each membrane tested; air-on 1, N_2-on 1, air-on 2 and N_2-on 2. Since no biochemical reactions took place and there were no respiring cells or biomass in the liquid used, the oxygen transfer rate was equal to the accumulation oxygen rate in the liquid and was given by the following (Garcia-Ochoa et al., 2010):

$$\frac{dC}{dt} = K_L a\,(C^* - C) \tag{3.3}$$

where dC/dt is the accumulation rate of oxygen in the liquid; $K_L a$ is the volumetric mass transfer coefficient; and C^* is the saturation concentration of oxygen in the liquid. The above equation was integrated and linearized to the following equation:

$$ln\frac{C^* - C_L}{C^* - C_o} = -K_L a\,.\,t \tag{3.4}$$

where C_o is the initial DO concentration; and C_L is the measured DO concentration in at time, t. The above equation was plotted with the slope equal to $K_L a$. The specific interfacial area, a, was directly determined by the following:

$$a = \frac{S_M}{V_L} \tag{3.5}$$

where a is the specific interfacial area; S_M is the exposed surface area of the membrane; and V_L is the volume of liquid in the liquid compartment. Since a can be easily determined for this module, K_L was separately be determined to compare the effect of the various membrane parameters on the oxygen mass transfer. Each trial was performed three times to generate 12 cycles in total, where the mean value of K_L was plotted and the error was determined by dividing the standard deviation by the mean of the 12 cycles.

3.2 Results and Discussion

3.2.1 Liquid flow structure in and around the membranes

The results of this study will be explained on the basis of the boundary layer structure of the fluids. Figure 3.2 shows the simplified structure of the fluids (liquid and gas) inside and surrounding the membrane.

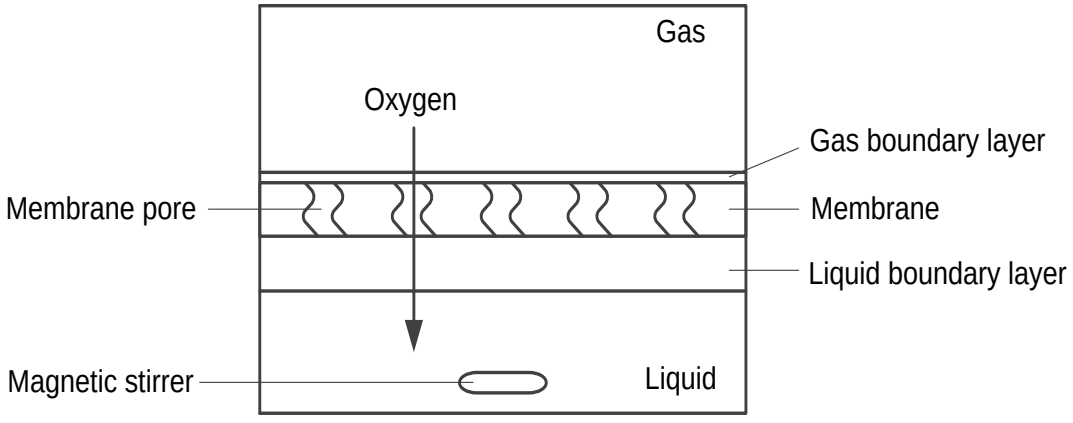

Figure 3.2. Boundary layers on the membrane

The gas and liquid film boundary layers are formed on the gas and liquid sides of the membranes, respectively. In the case of low solubility gases, the liquid film layer is limiting the mass transfer rate, and therefore, we will discuss here mainly the liquid structure inside and surrounding the membrane. The structure of the liquid film is different for the hydrophobic and the hydrophilic membranes.

When the membrane is hydrophilic, its pores are filled with liquid. Therefore, there are two liquid films which control the rate of oxygen mass transfer. The first film has a constant thickness (equal to the membrane thickness) and is represented by the liquid entrapped inside the membrane pores. The second film is the boundary layer outside of the membrane, whose thickness is a strong function of the hydrodynamic conditions of the liquid (mostly due to mixing). The thicknesses of these two films are of the same order of magnitude.

In the case of a hydrophobic membrane, the membrane pores are filled with a gas, and therefore, there is only one liquid film controlling the oxygen mass transfer – the boundary layer outside of the membrane.

The above two liquid structures will be used below to explain the effect of different parameters on the mass transfer coefficient of oxygen.

3.2.2 Probe lag and response time

The probe's membrane adds a lag and it was necessary to evaluate the time delay and its effect on the estimation of $K_L a$ values for the tested membranes. By subjecting the probe to instantaneous changes in DO concentration, the probe's lag constant, τ, was found to

be 4.8 $\pm$ 0.2s. If the dimensionless product of K_La and the probe lag constant is less than 0.02, the magnitude of error in estimating the oxygen transfer rate is less than 1% (Philichi and Stenstrom, 1989). The magnitude of $\tau.K_La$ was found to range from 5.45 x 10^{-3} to 1.05 x 10^{-3} for the membranes tested. Therefore the error in K_La estimation was limited to less than 1% as the magnitude of $\tau.K_La$ was found to be less than 0.02 for each membrane tested. It was also found that the probe took 15 seconds to achieve 95% of its steady-state value.

3.2.3 Oxygen mass transfer determination

All of the microporous membranes tested enabled oxygen transfer to the liquid compartment. According to the results from the air-on and air-off cycles, a typical curve is shown in Figure 3.3, from measuring the DO concentration over time.

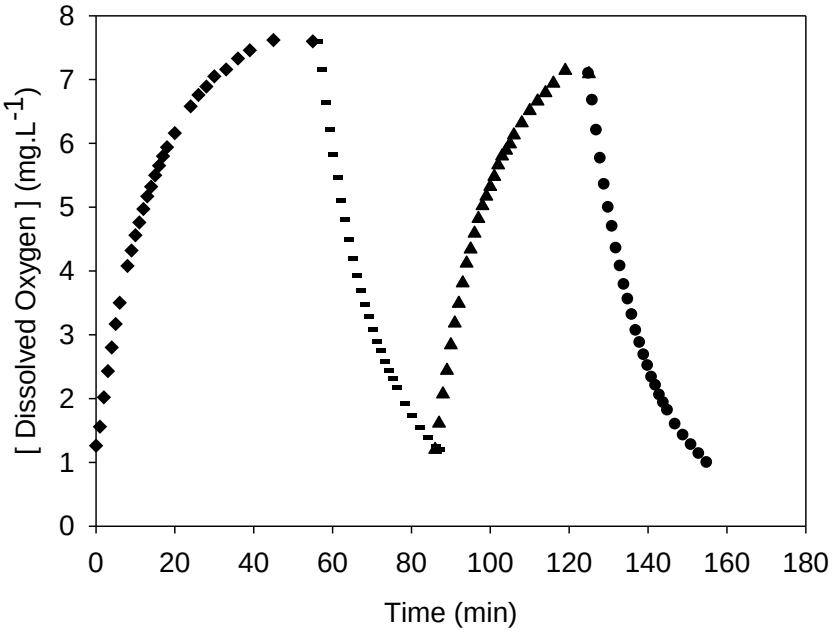

Figure 3.3. Air-on Air-off cycles for hydrophobic Polypropylene, with pore size 0.1µm, at 700RPM and 24°C. ♦Air-on 1; –Nitrogen-on 1; ▲Air-on 2; •Nitrogen-on 2

By linearization (Equation 3.4), a typical curve is shown in Figure 3.4, where $K_L a$ was determined from the slope.

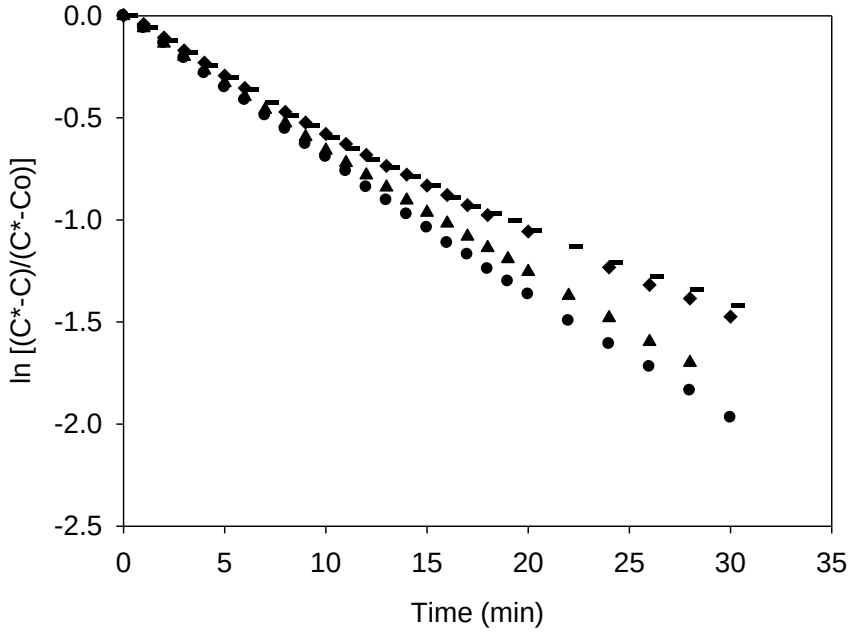

Figure 3.4. Linearization to determine the K_La for hydrophobic Polypropylene, with pore size 0.1µm, at 700RPM and 24°C. ♦Air-on 1; ▲Nitrogen-on 1; –Air-on 2; •Nitrogen-on 2

The R^2 factor was found to be greater than 0.98 for each trial which showed that the method of measurement in determining the K_La was quite precise. Each trial was repeated 3 times and the error was found to be within ±1.8% in the cases of the hydrophobic membranes studied, and within ±2.9% for the hydrophilic membranes. The greater error produced in the hydrophilic membranes was due to the occurrence of an initial uncontrolled liquid layer on the membrane in the gas compartment. While filling the liquid compartment in the module that had hydrophilic membranes, a small amount of liquid penetrated the membranes and formed a very small liquid layer in the gas compartment. This liquid layer was evaporated over time and depending on the amount of

liquid that penetrated and the thickness of the liquid film, variations occurred in the results.

3.2.4 Effect of agitation speed on K_L

The effect of the agitation speed on K_L was studied. For the case of hydrophilic membranes, as the rotational speed increased, the K_L values first increased, and then reached a plateau after a rotational speed of approximately 700 RPM as illustrated in Figure 3.5.

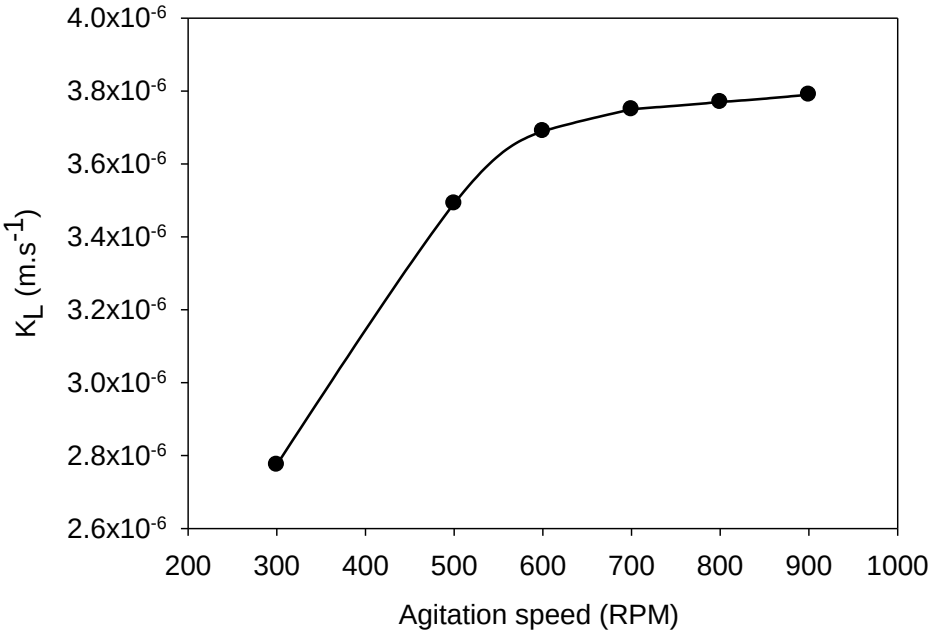

Figure 3.5. Effect of mixing speed on K_L of hydrophilic Nylon-6,6 with pore size 0.45µm, at 24°C

This effect can be explained on the basis of the liquid structure described above. As the rotational speed of the mixer increased up to 700 RPM, the thickness of the liquid

boundary layer was reduced and resulted in increasing K_L values. Therefore, it was assumed that under these conditions both the liquid layers (inside of the membrane and the boundary layer) are affecting the mass transfer rate as they probably have a similar thicknesses. However, the nearly constant values of K_L at rotational speeds above 700 RPM indicate that the thickness of the liquid boundary layer decreased so much that it became significantly smaller than the thickness of the membrane. Since the thickness of the static liquid film inside the membrane pores is unaffected by the liquid mixing, the mass transfer coefficients remained constant at high mixing speeds. Thus, in order to correctly determine the K_L of only the membrane, we worked at agitation speeds equal to or greater than 700RPM.

For the case of hydrophobic membranes, there was no plateau observed up to 900RPM, as depicted in Figure 3.6.

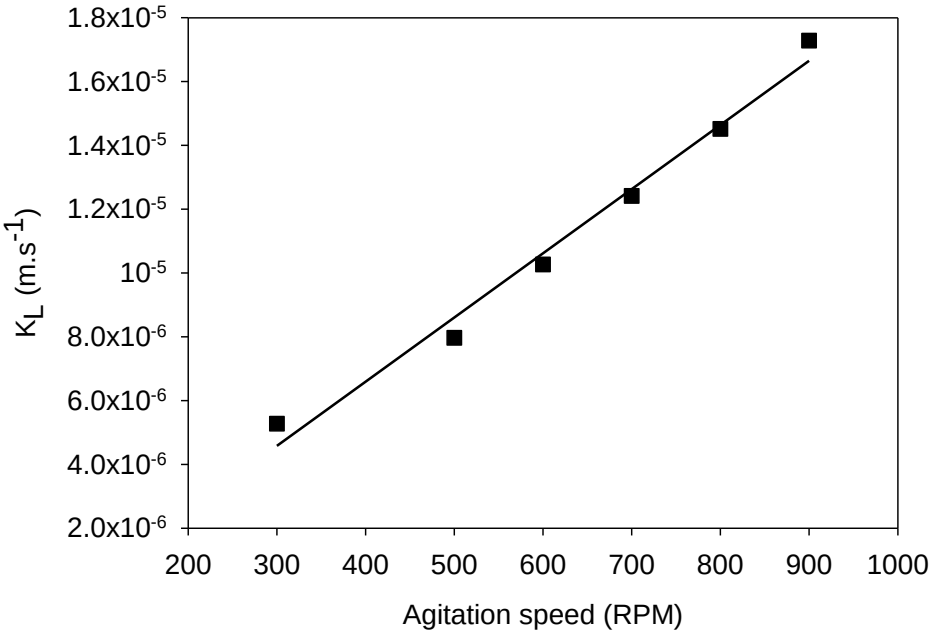

Figure 3.6. Effect of mixing speed on K_L of hydrophobic Polypropylene, with pore size 0.45µm, at 24°C

The pores of hydrophobic membranes are filled with gas and the only resistance to oxygen mass transfer was found in the liquid boundary layer which is strongly affected by the intensity of liquid mixing. A direct proportionality between the agitation speed and K_L values support that assumption. Thus, we chose to work at an agitation speed of 700RPM for the other experiments.

The liquid boundary layer thickness is inversely proportional to the liquid agitation rate and can be approximated by being equal to $\sqrt{(\nu/\Omega)}$ for a rotating disk, where ν is the kinematic viscosity of water, and Ω is the rotational velocity (Zoueshtiagh et al., 2003). A similar analysis was found for the approximate boundary layer thickness for a rotating fluid (Schlichting, 1979). The rotational velocity was calculated from the liquid agitation

speed as it is directly proportional to it and thus, the liquid boundary layer thickness decreased as the agitation speed is increased. This is effect is demonstrated in Figure 3.7.

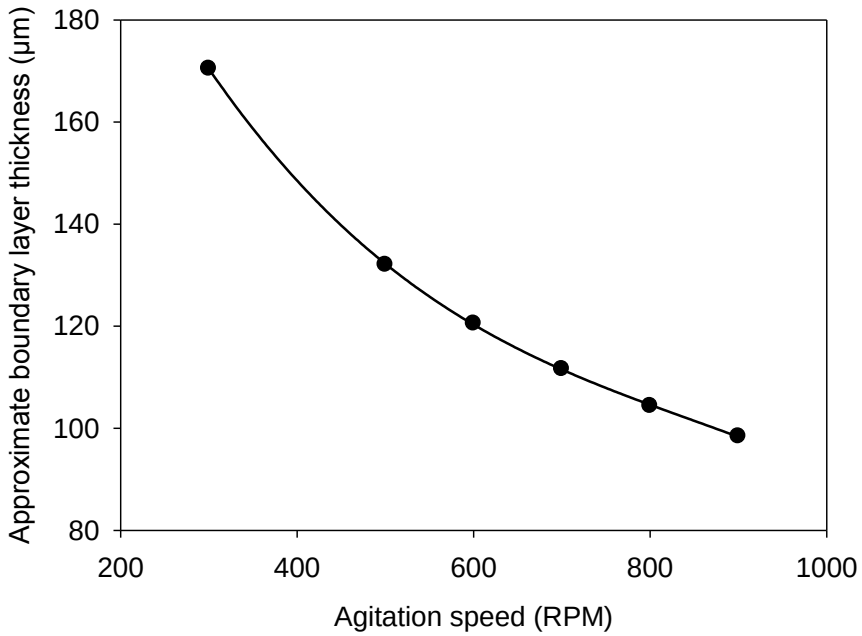

Figure 3.7. Effect of mixing speed on the approximate boundary layer thickness

According to the estimation of boundary layer thickness, a similar result was obtained when the boundary layer thickness was estimated as being approximately equal to $\sqrt{(vL/U)}$ for a flat plate, where L is the distance of the plate, and U is the liquid velocity, which is proportional to and can be calculated from the liquid agitation rate (Schlichting, 1979). It is important to note that, these estimations of the liquid boundary layer thickness are over-approximations as they do not take into account the roughness of the membrane surface. However in all cases that can be applied to the module in this study, the liquid boundary layer thickness is ultimately inversely proportional to the liquid agitation rate.

3.2.5 Determination of the oxygen mass transfer coefficient using different membranes

The K_L of each membrane at an agitation speed of 700RPM, temperature of 24^{o}C and gas flowrate of 100L.h^{-1} was determined and the results summarized in Table 3.2.

Table 3.2. Parameters and K_L observed for membranes at 24^{o}C and 700RPM

Material	Type	Pore size, µm	K_L x 10^5, m.s^{-1}
Polypropylene	Hydrophobic	0.10	1.279
Polypropylene	Hydrophobic	0.22	1.284
Polypropylene	Hydrophobic	0.45	1.288
PTFE	Hydrophobic	0.22	1.504
Polycarbonate	Hydrophobic	0.22	0.883
Polycarbonate	Hydrophobic	0.45	0.901
Polypropylene	Hydrophilic	0.45	0.361
Polyethersulfone	Hydrophilic	0.10	0.336
Polyethersulfone	Hydrophilic	0.45	0.289
Nylon-6,6	Hydrophilic	0.45	0.377
No membrane	-	-	0.839

3.2.6 Effect of hydrophobicity on oxygen mass transfer

In general, hydrophobic membranes were found to have higher oxygen mass transfer rates than the hydrophilic membranes (Table 3.2). For example, the hydrophobic polypropylene membrane had approximately 3.6 times higher K_L than the hydrophilic polypropylene membrane of the same pore size of 0.45μm. In the hydrophilic membranes, the pores were filled with water while in the hydrophobic they are filled with gas. The diffusivity of oxygen in water is very low as compared to the diffusion in air. This explains the higher mass transfer resistances that occurred with the hydrophilic membranes as there was an added mass transfer resistance due to the membrane, which resulted in lower K_L values. The choice of membrane material also affected the oxygen mass transfer rates. For the case of the hydrophobic membranes of the same pore size of 0.22 μm, the PTFE membrane had the highest K_L of 1.5×10^{-5} $m.s^{-1}$, followed by polypropylene and polycarbonate. This was partly due to the contact angle of the membranes which is a measure of the degree of hydrophobicity of the membranes. It was observed that as the contact angle increased and the more hydrophobic the membrane became, the K_L increased as illustrated in Figure 3.8.

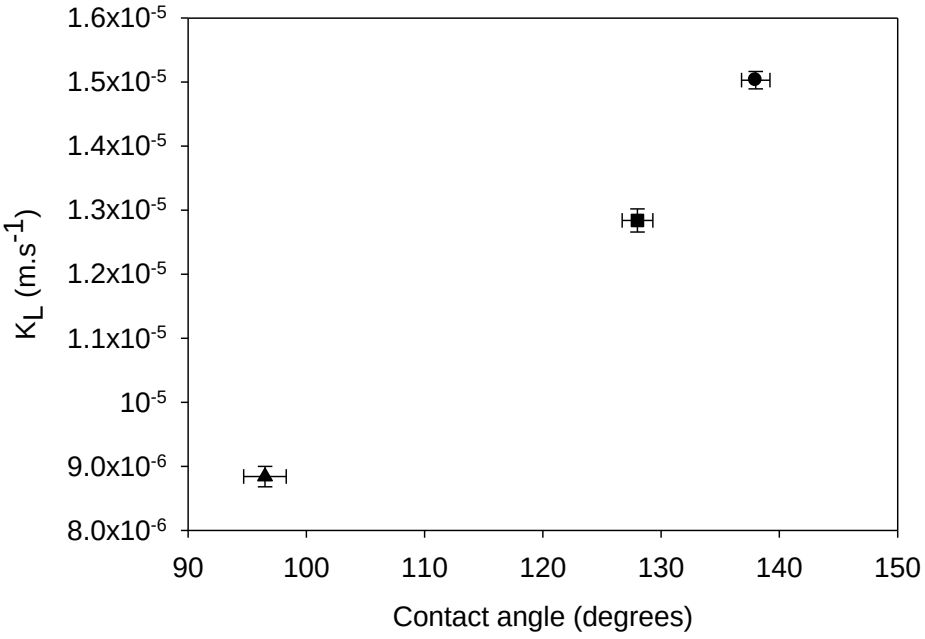

Figure 3.8. Effect of contact angle on hydrophobic membranes, with pore size 0.22µm. • PTFE; ■ Polypropylene; ▲ Polycarbonate

Since the diffusion of oxygen is through the pore system of microporous membranes, using membranes with a higher degree of hydrophobicity would result in higher oxygen mass transfer rates. The greater the hydrophobicity of the membranes, the higher the contact angle and thus a lower surface energy results (Quere, 2002). Having lower surface energy promotes a weaker liquid boundary layer formed on the membrane surface and thus an increase in the oxygen mass transfer rate as the resistance in the liquid boundary layer is reduced. As well as having the highest K_L, PTFE has many advantages as it can withstand many aggressive solvents and it is chemically and biologically inert, however it is costly and construction of a hollow fiber module made from PTFE may be expensive. Polypropylene is considered to be the cheaper alternative to PTFE and would make an

attractive choice of material to be used in construction of hollow fiber modules for oxygen mass transfer to bioprocesses.

3.2.7 Effect of surface roughness

The surface roughness of the hydrophobic membranes was found to increase as the hydrophobicity increased and is illustrated in Figure 3.9. However, this was only found to be in qualitative agreement and agrees well with literature as both hydrophobicity and hydrophilicity are reinforced by roughness but only qualitatively (Quere, 2002). Roughening of polymeric surfaces is one of the techniques used in fabrication of superhydrophobic membranes and the increase in surface roughness results in higher membrane hydrophobicity (Lv et al., 2011; Xue et. al., 2010). More air gets trapped in the microgrooves of the rougher membrane surfaces with the water droplets resting on the microportrusions which results in greater hydrophobicity (Xue et al., 2010). This also results in higher oxygen mass transfer as there is less water on the surface and a lower resistance from a weaker liquid boundary layer.

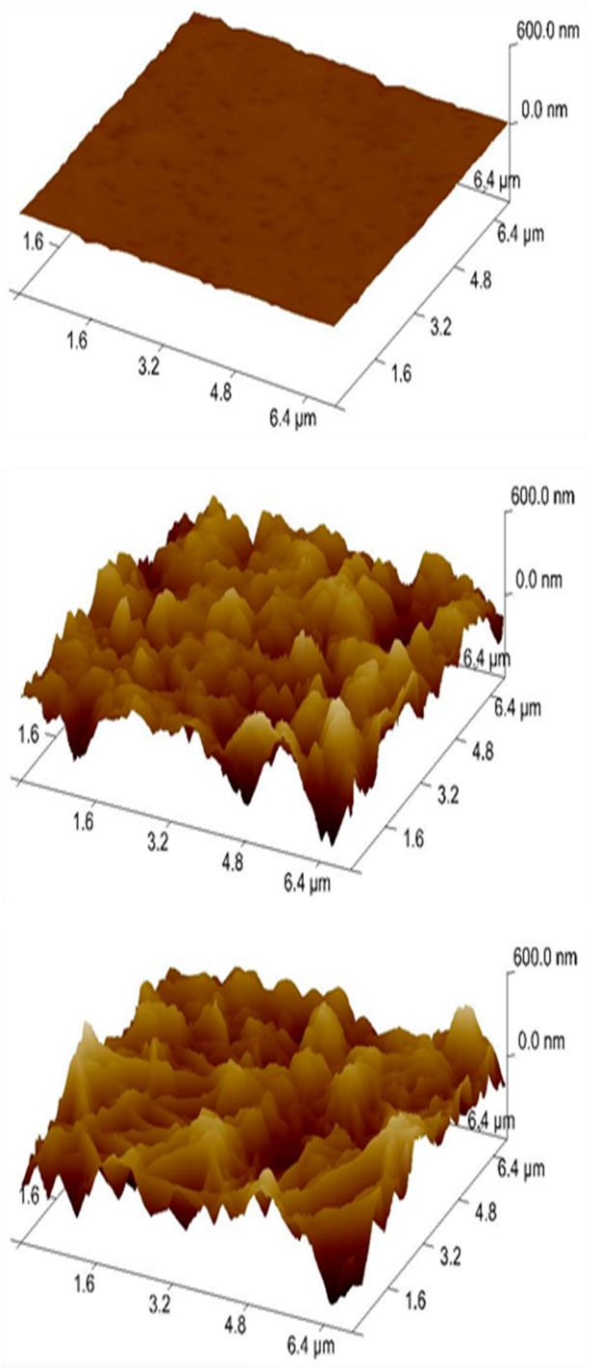

Figure 3.9. AFM surface images of 0.22µm hydrophobic membranes

3.2.8 Effect of membrane pore size on oxygen mass transfer

Different relations were observed for the effects of the pore size on the K_L values of the hydrophilic and hydrophobic membranes as depicted in Figure 3.10.

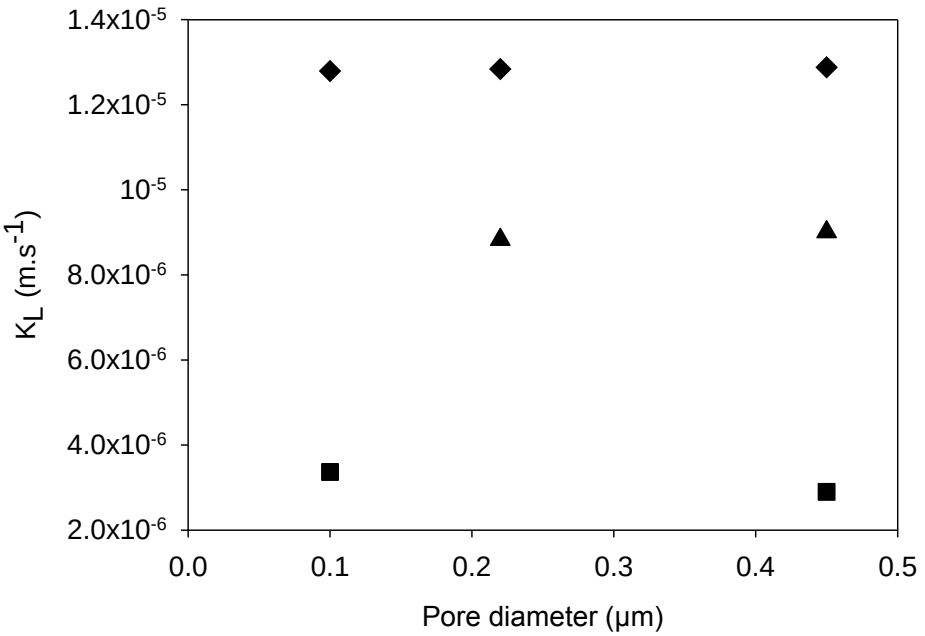

Figure 3.10. Effect of pore size on K_L of the membranes in de-ionized water at 24°C and 700RPM. ♦Hydrophobic Polypropylene; ▲ Hydrophobic Polycarbonate; ■ Hydrophilic Polyethersulfone

As the pore size increased in the hydrophilic polyethersulfone membranes, a decrease in K_L was observed. This was due to larger pores that held more water and more water being able to pass through the membrane during filling of the liquid compartment. This resulted in an increase in the mass transfer resistance of the hydrophilic polyethersulfone membranes.

As the pore size increased for the hydrophobic polypropylene membranes, only a very slight increase in K_L was observed, however this was found to be not statistically significant. A very slight increase in K_L was also observed for the hydrophobic polycarbonate membranes and this was also found to be not statistically significant. As a result, the effect of pore size on the hydrophobic membranes was considered negligible. This was due to the fact that the main resistance to oxygen mass transfer in the hydrophobic membranes lies in the liquid boundary layer and since the pores are occupied with gas, then the slight increase in gas mass transfer through larger pores would be negligible compared to the resistance in the liquid boundary layer. The advantage of hydrophobic membranes with smaller pore sizes is that they can withstand higher gas pressures without forming bubbles as they usually have higher bubble points. As a result, the hydrophobic membranes with smaller pore sizes would be suitable if the system has to be pressurized and they would still achieve desirable oxygen mass transfer rates.

3.2.9 Effect of the presence of membrane

In the case of the absence of the membrane, where air was allowed to contact directly the free surface of the liquid, a highly unexpected result was obtained. One would expect that when the gas and liquid are separated by a membrane, there will be an additional mass transfer resistance due to the membrane, and that the mass transfer coefficient will be lower than in the case of a direct gas-liquid contact. Contrary to that expectation, we found out that K_L in the case of gas and liquid separated by hydrophobic membranes was significantly larger than in direct gas-liquid contact as shown in Table 3.2.

However, the mass transfer coefficient in the case of hydrophilic membranes was smaller than in a direct gas-liquid contact (Table 3.2). These results can also be explained by the effect of the boundary layer thickness. As the free liquid surface is rotating, there is very little shear rate on the liquid side, which would result in a very thick boundary layer. However when a static membrane is present at the gas-liquid interface, the shear rate is much higher, and therefore the liquid boundary layer is significantly thinner than in the case of a membrane–free interface.

Since in the hydrophobic membranes the liquid boundary layer represents the only significant mass transfer resistance, and since it is much thinner than in a direct gas-liquid contact, the oxygen mass transfer in the hydrophobic membrane-separated fluids was higher than in the case of no membrane at all.

As mentioned above, in the case of hydrophilic membranes, the oxygen mass transfer is affected by both the liquid-side boundary layer and the static liquid film in the membrane pores. Therefore, the lower oxygen mass transfer rate compared to the direct gas-liquid contact is probably due to the fact that the combined thickness of the liquid film and the boundary layer in the case of hydrophilic membrane is more than the liquid boundary layer thickness surrounding the direct gas-liquid interface.

3.3 Flat module oxygen- bioreactor medium

Similar experiments were done with the setup and conditions specified in Section 3.1.2 but with the bioreactor solution obtained from the Biogenerator instead of de-ionized water to determine the behaviour of the membranes for oxygen mass transfer using this

liquid. Only the hydrophobic membranes were used with the properties already described in Section 3.1.1.

3.3.1 Preparation and measurement methods of the bioreactor solution

The bioreactor solution was obtained from the Biogenerator and contained ferric and ferrous iron sulphate with ~2% H_2SO_4. The ferric iron (Fe^{3+}) concentration was determined from titration with EDTA in acetic acid-sodium acetate buffer of pH ~2 at 60-70°C in the presence of 5-sulphosalicylic acid as a complexometric indicator. The ferrous iron (Fe^{2+}) concentration was determined by titration with K_2CrO_4 in ~10% H_2SO_4, with N-phenylanthranilic acid as a potentiometric indicator.

The pH of the solution was measured using an Orion 8012BN Ross combination pH electrode (Thermo Scientific) connected to an Orion 420A+ pH/mV meter (Thermo Scientific). A three-point calibration with pH 1.00, 2.00 and 3.00 buffers (Ricca Chemical Company, Arlington, TX, USA) was done at room temperature. An in-house H_2SO_4 solution with a known pH of 0.86 was used as a reference during the calibration.

The bioreactor solution was filtered with a 0.2 micron polyethersulfone filter (Pall Co.) to remove the *L. ferriphilum* to neglect the effect of microbial oxygen uptake and simplify measurements of K_La as it was done solely for comparison of the performance of the various membranes tested in this liquid. The solution was also heated afterwards to ~70^oC for 5 minutes to be certain that there were no living *L. ferriphilum* cells.

The measurements of DO concentration in the bioreactor solution had to be restricted to 7-8 minutes as there is a tendency for ferric irons to pass through the probe's membrane after that limit and get reduced at the platinum electrode which would result in probe failure (Penev, 2011). As a result, three trials of only an air-on cycle in each trial were used to determine K_L, with the mean value plotted with the standard deviation.

3.3.2 Results and Discussion

The effects of different hydrophobic membranes and their pore sizes on the liquid mass transfer coefficient of oxygen are illustrated in Figure 3.11 when a bioreactor solution of pH 0.9 with 48.9g.L^{-1} Fe^{3+} and 0.63g.L^{-1} Fe^{2+} was used.

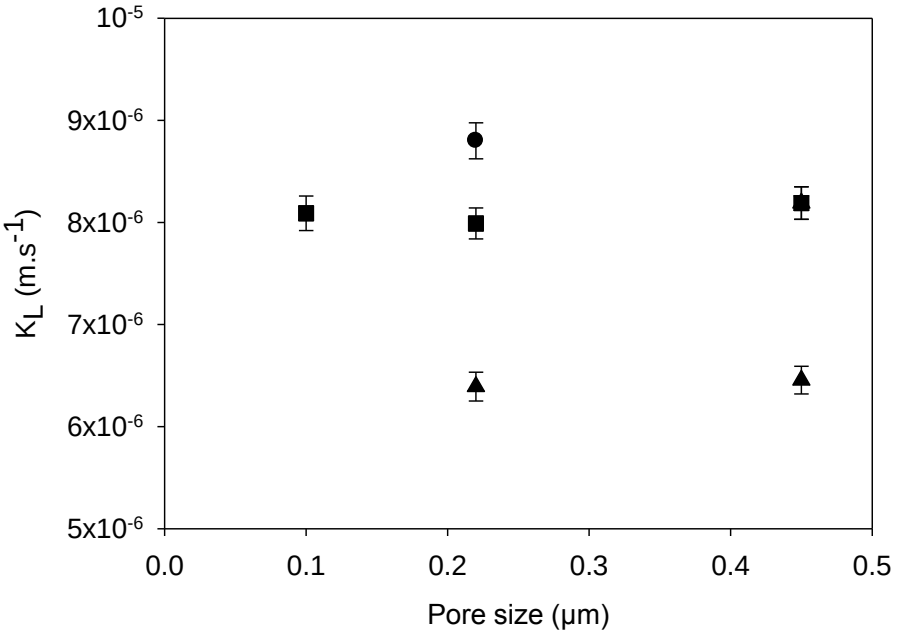

Figure 3.11. Oxygen mass transfer with the bioreactor solution in the flat module. • PTFE; ■ Polypropylene; ▲ Polycarbonate

The overall values of K_L were lower for the bioreactor solution as compared to that with water which was probably due to different liquid properties and increased density and viscosity which could result in a thicker liquid boundary layer and increased resistance to gas mass transfer. A similar behaviour was observed for the membrane material as the K_L generally increased as the hydrophobicity increased. This effect was less pronounced with the bioreactor solution owing to the differences in the surface tension of the liquid. As with de-ionized water, the effect of pore size was considered negligible as the limiting factor was the thickness of liquid boundary layer. Polypropylene only had a slightly lower K_L than PTFE and would make it a suitable choice for material selection for a hollow fiber module owing to its high chemical and thermal stability and relatively low cost.

3.4 Conclusions from flat membrane module experiments

- Surprisingly, it was found out that the oxygen mass transfer coefficient in the case when a gas and liquid are separated by a hydrophobic membrane is larger than in the case of a direct gas-liquid contact
- When the gas and liquid are separated by a hydrophilic membrane, the mass transfer coefficient is less than that in the case of a direct gas-liquid contact
- For the hydrophobic membranes, the increase in agitation speed resulted in an increase in K_L in an almost linear relationship, in the entire range of agitation speed studied in de-ionized water.
- The increase in agitation speed resulted in an increase in K_L and then reached a plateau after 700RPM for hydrophilic membranes.

- Hydrophobic membranes had approximately 3.6 times larger K_L than hydrophilic membranes for oxygen mass transfer in de-ionized water.
- The oxygen mass transfer rate increased as the degree of hydrophobicity of the membranes increased.
- Regarding the membrane material, PTFE had the highest K_L of 1.5 x 10^{-5}m.s^{-1} in de-ionized water.
- The effect of pore size was negligible for the hydrophobic membranes.
- Oxygen mass transfer decreased as the pore size was increased for the hydrophilic membranes.
- All of the above results can be explained by the thickness of the liquid boundary layer surrounding the membrane surface and its relation to the thickness of the membrane.

3.5 Nomenclature

a	specific interfacial area	m^{-1}
C	actual DO concentration	$g.L^{-1}$
C^*	saturation concentration of oxygen in the liquid	$g.L^{-1}$
C_L	measured DO concentration	$g.L^{-1}$
C_o	initial DO concentration	$g.L^{-1}$
C_p	DO concentration indicated by the probe	$g.L^{-1}$
C_{po}	initial probe reading	$g.L^{-1}$

dC/dt	accumulation rate of oxygen in the liquid	$g.L^{-1}.s^{-1}$
K_La	volumetric mass transfer coefficient	s^{-1}
S_M	exposed surface area of the membrane	m^2
t	time of trial	s
U	liquid velocity	$m.s^{-1}$
V_L	volume of liquid in the liquid compartment	m^3

Greek letters:

Ω	rotational velocity	$rad.s^{-1}$
τ	probe lag constant	s
ν	kinematic viscosity of water	$m^2.s^{-1}$

Chapter 4 : Flat module- Carbon dioxide mass transfer

The study of carbon dioxide mass transfer in water was somewhat different compared to oxygen mass transfer in water. Measuring the dissolved carbon dioxide concentration is slightly more complicated. Carbon dioxide is more soluble than oxygen in water. Also, carbon dioxide chemically reacts with water to form a weak carbonic acid according to the following:

$$CO_2 + H_2O \leftrightarrows H_2CO_3 \quad (4.1)$$

The carbonic acid dissociates into the bicarbonate ion according to the following:

$$H_2CO_3 \leftrightarrows HCO_3^- + H^+ \quad (4.2)$$

The bicarbonate dissociates into the carbonate ion given by:

$$HCO_3^- \leftrightarrows CO_3^{2-} + H^+ \quad (4.3)$$

At pH greater than 10.4, the carbonate (CO_3^{2-}) form becomes the most predominant. At pH above 6.5, the bicarbonate (HCO_3^-) form predominates. At pH 5 and below, almost all of the carbon dioxide is converted to the dissolved CO_2 form (Blanch and Clark, 1997). Therefore to efficiently measure the effect of dissolved CO_2, the pH of the system should be maintained below 5. The value of K_L will be pH dependant and can also be adjusted to any pH according to the following (Aptel and Semmens, 1996):

$$K_L = K_{L,measured} \left(1 + \frac{[H^+]}{K_a}\right) \quad (4.4)$$

where K_L is the liquid mass transfer coefficient for carbon dioxide at any pH; $K_{L,measured}$ is the measured value of the liquid mass transfer coefficient at the measured pH; and K_a is the dissociation constant of carbon dioxide.

The flat membrane module described in Chapter 3 was used to fundamentally determine the effects of agitation, membrane material, hydrophobicity, pore size and the effect of the membrane itself on the liquid mass transfer coefficient of carbon dioxide, K_L, by bubble-free gas transfer. In the first part (Sections 4.1 and 4.2) a liquid consisting of de-ionized water with a 10% vol. carbon dioxide buffer solution was used so that the pH would be maintained below 5 to ensure that almost all the carbon dioxide would be in the dissolved carbon dioxide form and probe interferences would be minimized. The second part (Section 4.3) consists of experiments with the carbon dioxide buffer as the liquid solution to maintain the pH at 4.5.

4.1 Materials and Methods

4.1.1 Membrane parameters

The flat sheet membranes used in this study were the hydrophobic polypropylene (0.1µm, 0.22µm and 0.45µm), PTFE (0.22µm), polycarbonate (0.22µm and 0.45µm) and the hydrophilic polypropylene (0.45µm), with their properties already listed earlier in Section 3.1 of Chapter 3.

4.1.2 Experimental setup

The experimental setup used in this study is depicted in Figure 4.1.

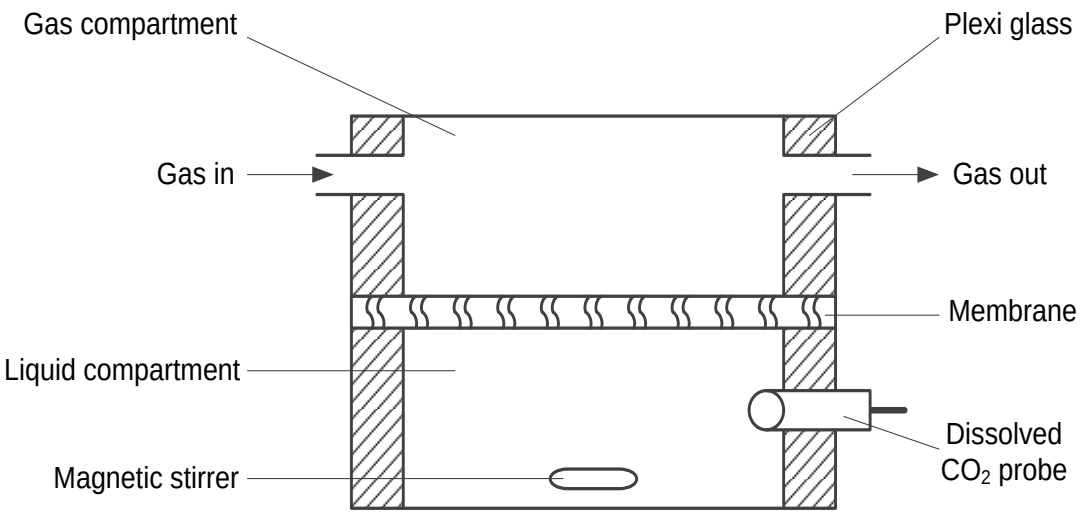

Figure 4.1. Experimental setup for flat module carbon dioxide mass transfer

The exposed geometrical surface area of the membranes was 8.04cm^2. The volumes of the liquid and gas compartments were 12.1cm^3 each. A 0.5 inch magnetic stir bar (VWR) was used for agitation in the liquid compartment. The liquid used was de-ionized water with a 10% vol. of a carbon dioxide buffer solution ISE-8750-R1 (Omega, Stamford, CT, USA), to maintain the pH of the liquid at 4.89 for the probe to efficiently measure dissolved carbon dioxide. Carbon dioxide gas (Praxair Canada, Mississauga, Ontario) was supplied to the gas compartment at a flowrate of 250mL.min^{-1} using high precision rotameters (Omega). Nitrogen (95%), (Praxair Canada) was used to sparge the liquid of carbon dioxide before filling the liquid compartment in each experiment. The flow-through module maintained the gas pressure at near atmospheric and below the bubble point of the membranes. The dissolved carbon dioxide concentration in the liquid was measured with a dissolved carbon dioxide probe ISE-8750 (Omega) connected to an Accumet Excel XL 15 pH/mV/temperature meter (Fischer Scientific, Ottawa, Ontario). To convert the mV readings to concentration values, a three point calibration was done

for the probe using serial dilutions of a 1000ppm carbon dioxide standard ISE-8750-S2 (Omega) to obtain 10ppm, 100ppm and 1000ppm carbon dioxide concentrations for the calibration curve. The liquid temperature was maintained at 24^{o}C.

4.1.3 Calculation of K_L

The liquid solution was first sparged with nitrogen to a near zero carbon dioxide concentration and transferred to the liquid compartment and sparged again. The carbon dioxide gas flow was turned on at 250mL.min^{-1} and the dissolved carbon dioxide concentration was monitored over time at a set stirrer speed. The dynamic method was carried out to determine K_L of carbon dioxide, using the same procedure outlined in Section 3.1.4. However, the nitrogen on cycle was not utilized in order to minimize the error in the event of a minute amount of bicarbonate ions that would not be able to be sparged from the system. Each trial was repeated for a total of three CO_2-on trials by re-filling the liquid compartment with a newly sparged liquid solution.

4.2 Results and Discussion

All of the microporous membranes tested enabled carbon dioxide mass transfer to the liquid compartment. A typical curve is shown in Figure. 4.2, from measuring the dissolved carbon dioxide concentration over time.

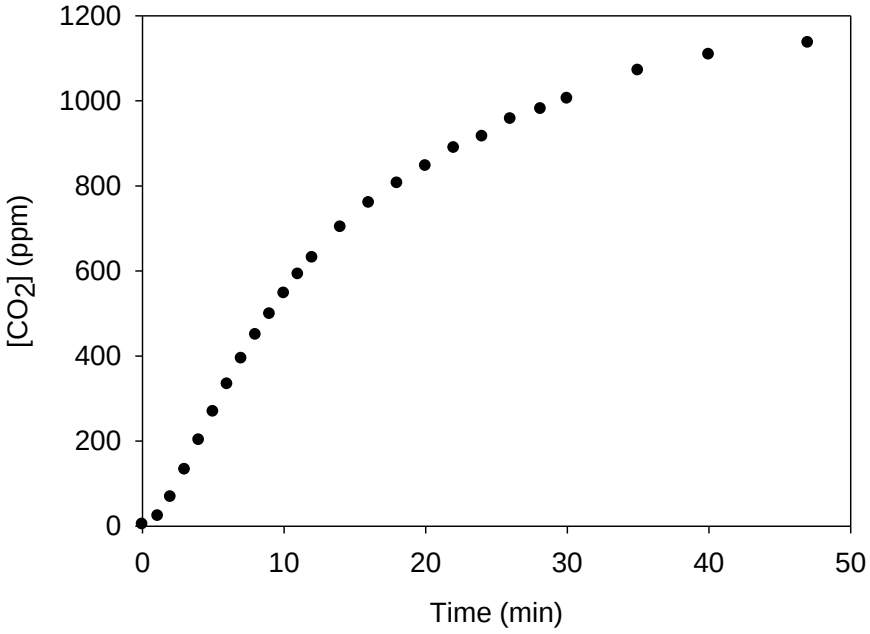

Figure 4.2. CO_2 on cycle for hydrophobic Polypropylene, with pore size 0.45µm at 900RPM

By linearization (Equation 3.4), a typical curve is shown in Figure 4.3, where $K_L a$ was determined from the slope.

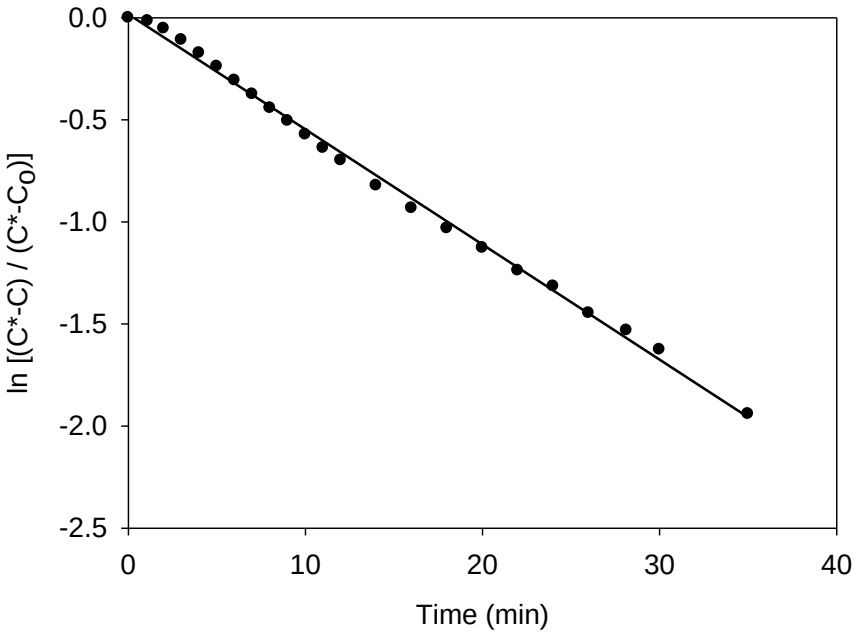

Figure 4.3. Linearization to determine the K_La for hydrophobic Polypropylene, with pore size 0.45µm at RPM 900

The R^2 factor was found to be greater than 0.98 for each trial which showed that the method of measurement in determining the K_La was quite precise. Each trial was done 3 times and the error was found to be within ±2.1% in the cases of the hydrophobic membranes studied, and within ±3.3% for the hydrophilic membranes. The greater error produced in the hydrophilic membranes was due to a small amount of liquid penetrating the membrane during filling.

4.2.1 Effect of Agitation

The effect of the agitation speed on K_L was studied. For the case of hydrophilic membranes, as the rotational speed increased, the K_L values first increased, and then

reached a plateau after a rotational speed of approximately 700 RPM as illustrated in Figure 4.4.

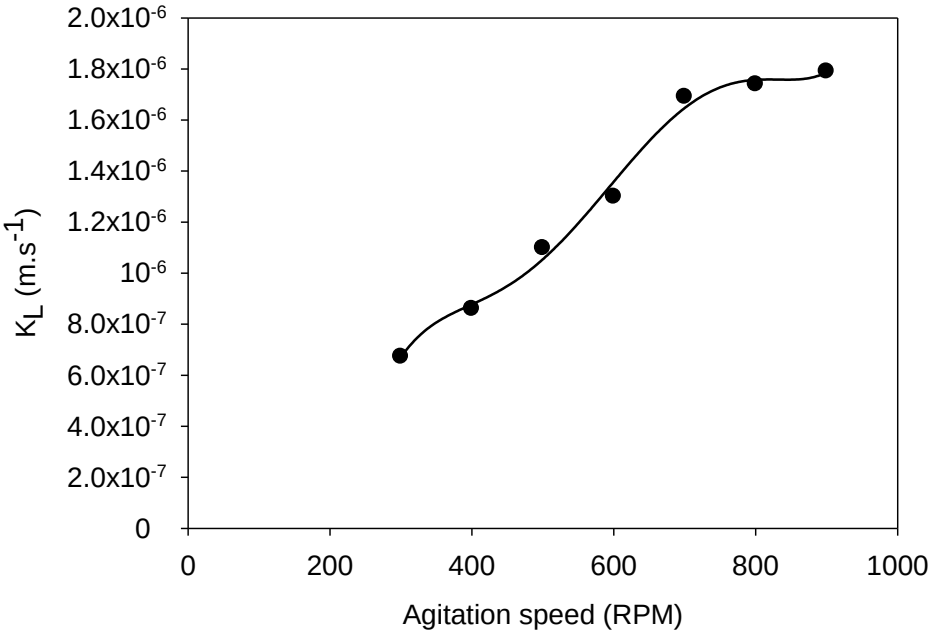

Figure 4.4. Effect of mixing speed on K_L of hydrophilic polypropylene with pore size 0.45µm, at 24°C

A slightly similar result was noticed when compared to the oxygen mass transfer and this is also due to the reduction of the liquid boundary layer thickness until it became negligible compared to the thickness of the membranes. As with the oxygen mass transfer results, for the case of hydrophobic membranes, as the pores were gas filled, there was no plateau observed up to 900RPM. This is depicted in Figure 4.5.

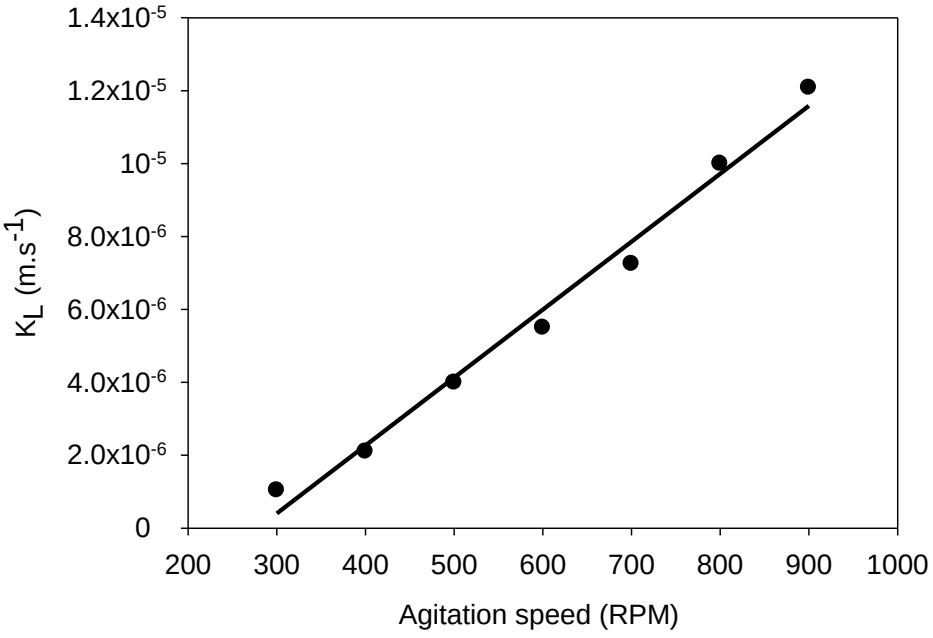

Figure 4.5. Effect of mixing speed on K_L of hydrophobic Polypropylene, with pore size 0.45µm, at 24°C

A direct proportionality between the agitation speed and K_L values was found and is explained by the reduction of the liquid boundary layer as the agitation is increased thereby reducing the resistance to carbon dioxide transfer almost linearly. Thus, we chose to work at an agitation speed of 700RPM for the other experiments. The hydrophobic polypropylene membrane was found to have approximately 4.2 times greater K_L than the hydrophilic polypropylene at 700 RPM. Since the pores are gas filled in the hydrophobic membranes, there is less resistance to carbon dioxide mass transfer as when the pores are liquid filled.

4.2.2 Determination of the liquid mass transfer coefficient for carbon dioxide using different membranes

The K_L of each membrane at an agitation speed of 700RPM, temperature of 24^{o}C and carbon dioxide gas flowrate of 250mL.min^{-1} was determined and the results summarized in Table 4.1.

Table 4.1. Parameters and K_L observed for membranes at 24^{o}C and 700RPM

Material	Type	Pore size, µm	K_L x 10^{6}, m.s^{-1}
Polypropylene	Hydrophobic	0.10	7.25
Polypropylene	Hydrophobic	0.22	7.35
Polypropylene	Hydrophobic	0.45	7.29
PTFE	Hydrophobic	0.22	8.35
Polycarbonate	Hydrophobic	0.22	4.83
Polycarbonate	Hydrophobic	0.45	4.97
Polypropylene	Hydrophilic	0.45	1.69
Polyethersulfone	Hydrophilic	0.10	1.63
Polyethersulfone	Hydrophilic	0.45	1.42
No membrane	-	-	4.32

It was also noticed that generally the K_L values for carbon dioxide were lower than the K_L values for oxygen (Chapter 3). This can be explained by the lower diffusion coefficient of carbon dioxide in water (≈1.6 x 10^{-5} cm^{2}.s^{-1}) as compared to oxygen in water (≈2 x 10^{-5} cm^{2}.s^{-1}). The lower K_L values can also be attributed to the fact that salts were present in

the liquid used in the carbon dioxide experiments as a carbon dioxide buffer was added to the de-ionized water which would reduce the mass transfer and lower the pH.

4.2.3 Effect of membrane material and parameters

It was observed that K_L in the case of gas and liquid separated by hydrophobic membranes was significantly larger than in direct gas-liquid contact (with no membrane) as shown in Table 4.1. However, the mass transfer coefficient in the case of hydrophilic membranes was smaller than in a direct gas-liquid contact (Table 4.1). These results can also be explained by the effect of the boundary layer thickness as the static membranes add a liquid boundary layer at the gas-liquid interface, the shear rate is much higher, and therefore the liquid boundary layer is significantly thinner than in the case of a membrane–free interface. In the case of the hydrophobic membranes, the liquid boundary layer represents the only significant mass transfer resistance to carbon dioxide, and since it is much thinner than in a direct gas-liquid contact, the carbon dioxide mass transfer in the hydrophobic membrane-separated fluids was higher than in the case of no membrane at all.

In the case of hydrophilic membranes, the lower carbon dioxide mass transfer rate compared to the direct gas-liquid contact is probably due to the fact that the combined thickness of the liquid film inside the pores and the boundary layer is more than the liquid boundary layer thickness surrounding the direct gas-liquid interface of no membrane.

The choice of membrane material affected the carbon dioxide mass transfer rates due to the hydrophobicity of the membranes. For the case of the hydrophobic membranes of the same pore size of 0.22 µm, the PTFE membrane had the highest K_L of 8.34 x 10^{-6} m.s^{-1},

followed by polypropylene and polycarbonate. It was observed that as the water contact angle increased and the more hydrophobic the membrane became, the K_L increased as illustrated in Figure 4.6.

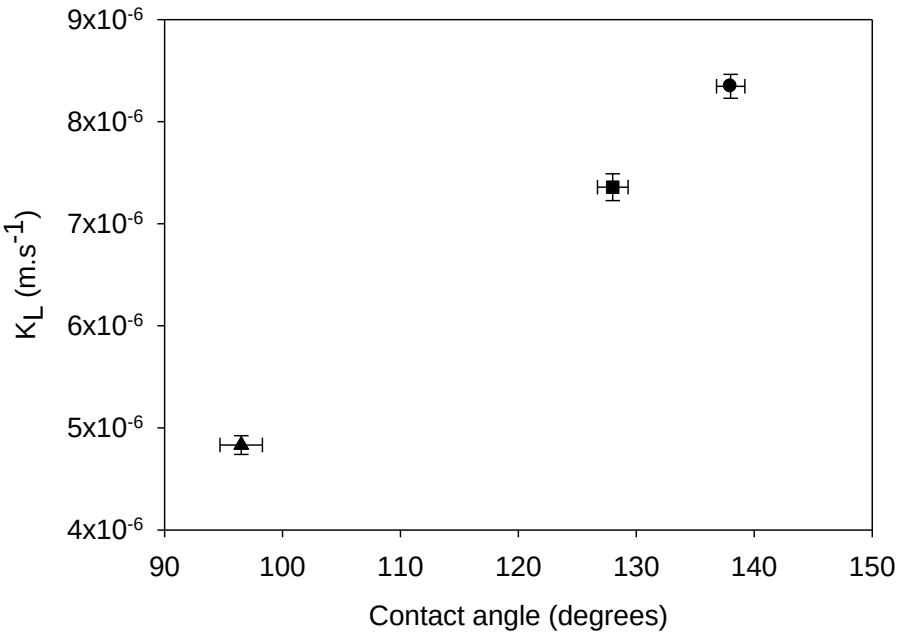

Figure 4.6. Effect of hydrophobicity on hydrophobic membranes, with pore size 0.22µm. • PTFE; ■Polypropylene; ▲Polycarbonate

As the diffusion of carbon dioxide is through the pore system of microporous membranes, using membranes with a higher degree of hydrophobicity would result in higher carbon dioxide mass transfer rates as more gas would be trapped in the pores which would mean a lower resistance to mass transfer and a weaker liquid boundary layer.

The effect of the pore size on the K_L was found to be negligible of the hydrophobic membranes. This was due to the fact that the main resistance to carbon dioxide mass transfer lies within the liquid boundary layer as the pores are gas filled, and would be

completely dependent on the hydrodynamic conditions of the system. However, K_L slightly decreased as the pore size increased for the hydrophilic membranes. This was due to more liquid being present in the pores which would increase the resistance to carbon dioxide mass transfer. This result is depicted in Figure 4.7.

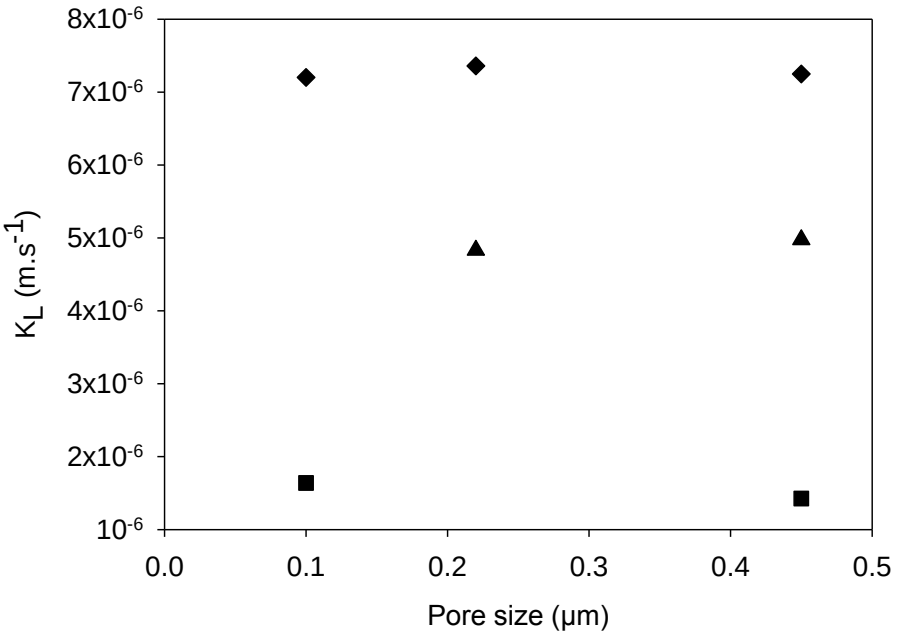

Figure 4.7. Effect of pore size on K_L of the membranes at 24°C and 700RPM. ♦Hydrophobic Polypropylene; ▲ Hydrophobic Polycarbonate; ■ Hydrophilic Polyethersulfone

Similar relationships were obtained for the carbon dioxide mass transfer in the membranes studied when compared to the oxygen mass transfer results which proves that the bubble-free gas transfer using microporous membranes is not gas specific for low soluble gases in water as the transfer is mainly though the pore system of the membrane. Thus, unlike dense membranes, there is no gas selectivity when using microporous

membranes as gas-liquid contactors for dissolved oxygen and carbon dioxide in water. The limiting factor of bubble-free gas transfer would be the liquid boundary layer and economically reducing it would be the main goal for any bubble-free process; whether it be by using more hydrophobic membranes or improving the hydrodynamics.

4.3 Flat module carbon dioxide mass transfer with buffer solution

Similar experiments were done with the setup and conditions specified in Section 4.1.2 but with only the carbon dioxide buffer solution ISE-8750-R1 (Omega) as the liquid to determine the behaviour of the membranes for carbon dioxide mass transfer using this liquid which is kept at a constant pH of 4.5. The results are illustrated in Figure 4.8.

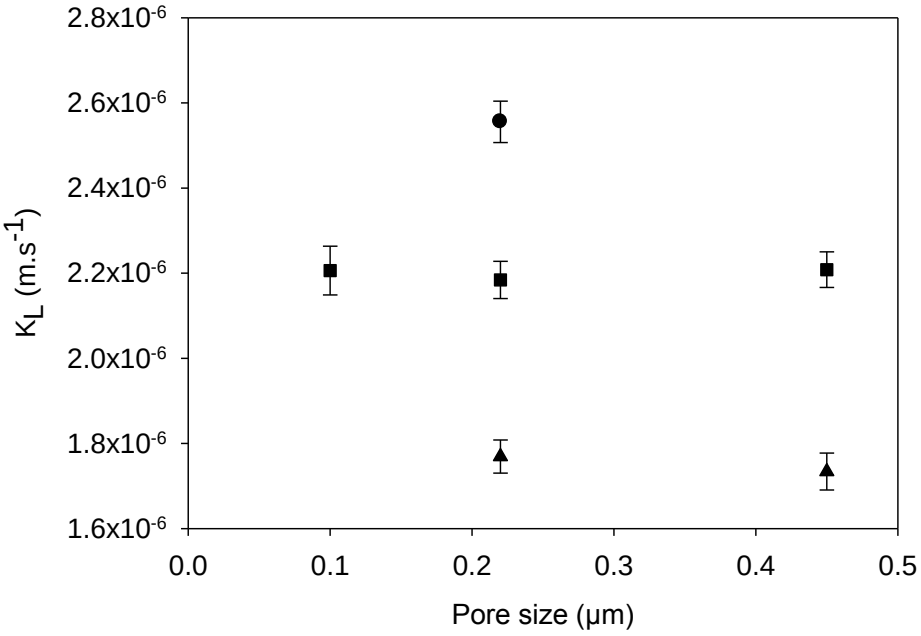

Figure 4.8. Carbon dioxide mass transfer with carbon dioxide buffer solution pH4.5. • PTFE; ■Polypropylene; ▲Polycarbonate

The same relationships were obtained for the K_L of the membranes with the carbon dioxide buffer solution as with the de-ionized water with 10% vol. buffer solution. The effect of pore size was negligible on carbon dioxide mass transfer and the increase in hydrophobicity resulted in an increase in carbon dioxide mass transfer. However, this effect was less pronounced owing to different liquid properties and more salts in the media used which resulted in slightly lower K_L values.

4.4 Conclusions from flat module experiments

- Microporous membranes are not gas specific during bubble-free gas transfer for dissolved carbon dioxide and oxygen in water as similar relationships were obtained in both cases.

- The hydrodynamics and properties of the liquid influence the carbon dioxide mass transfer due to the effects of the liquid boundary layer on the membrane.
- Greater hydrophobicity improved carbon dioxide mass transfer.
- PTFE had the highest K_L of 8.34 x 10^{-6} m.s^{-1}.

Chapter 5 : Hollow fiber- bubble-free oxygen mass transfer

As stated earlier in Chapter 1, microporous hollow fiber membrane modules as gas-liquid contactors present many advantages over conventional bubbling for aeration in bioreactors. Hollow fibers have the ability to pack very large membrane areas into small modules (Baker, 2004). Increased interfacial areas associated with hollow fiber modules enable higher oxygen mass transfer rates. Drawing from the results of Chapter 3, polypropylene is a suitable candidate for membrane material in a hollow fiber module for usage in bubble-free aeration. Polypropylene also has a broad chemical compatibility due to its excellent chemical resistance as it has the ability to withstand many aggressive solvents and solutions. This makes polypropylene suitable for long term usage in the low pH solution of the Biogenerator. The pore size was found in Chapter 3 to have a negligible effect on the oxygen mass transfer rate, however lower pore sizes have greater bubble points and would be advantageous to use in these modules to prevent any bubble formation from occurring.

In the case of the Biogenerator, previous researchers have shown that increasing the oxygen mass transfer does increase the performance of the system as the oxidation rate of ferrous irons by *Leptospirillum ferriphilum* is higher, however this required greater energy input as higher air flowrates and agitation was necessary. In the case of bubbling, greater depths in bioreactors produce a higher hydrostatic head and will require greater power input. In bubble-free aeration with hollow fiber modules, the pressure drop between the modules can be evaluated and the approximate power input to this system can be computed and compared to bubbling to determine which process is more energy

efficient. This is a critical parameter to determine as the Biogenerator basically produces electrical energy, therefore, increasing the performance with a reduced energy input is one of the main goals to increase the efficiency of this system.

The main goals of this chapter are to determine the volumetric mass transfer coefficient, $K_L a$, for bubble-free aeration with a hollow fiber module at various liquid flowrates and compare this to bubbling under the same conditions. The effect of recirculating the liquid in the shell side of the module and in the lumen side will also be investigated to compare the difference in performance. The approximate power input at the different liquid flowrates in the hollow fiber module will be compared to the power input of bubbling. The liquid used in the first part (Sections 5.1 and 5.2) of this chapter was de-ionized water. In the second part of this chapter (Section 5.3), the bioreactor solution from the Biogenerator was used as the liquid solution.

5.1 Materials and Methods

5.1.1 Membrane module

The hollow fiber module used in this study was a Liqui-Cel® 1 x 5.5 MiniModule® (Membrana, Charlotte, NC, USA). The properties of this membrane module are listed in Table 5.1.

Table 5.1. Hollow fiber membrane module parameters

Module Characteristic	Amount
Membrane material	Polypropylene X50 fiber
Pore size	0.04µm
Porosity	40%
Fiber internal diameter	220µm
Fiber external diameter	300µm
Length of fiber	12cm
Number of fibers	2300
Effective surface area	$0.18m^2$
Volume inside fibers	16mL
Volume outside fibers	25mL

5.1.2 Experimental setup

The experimental setup is depicted in Figure 5.1.

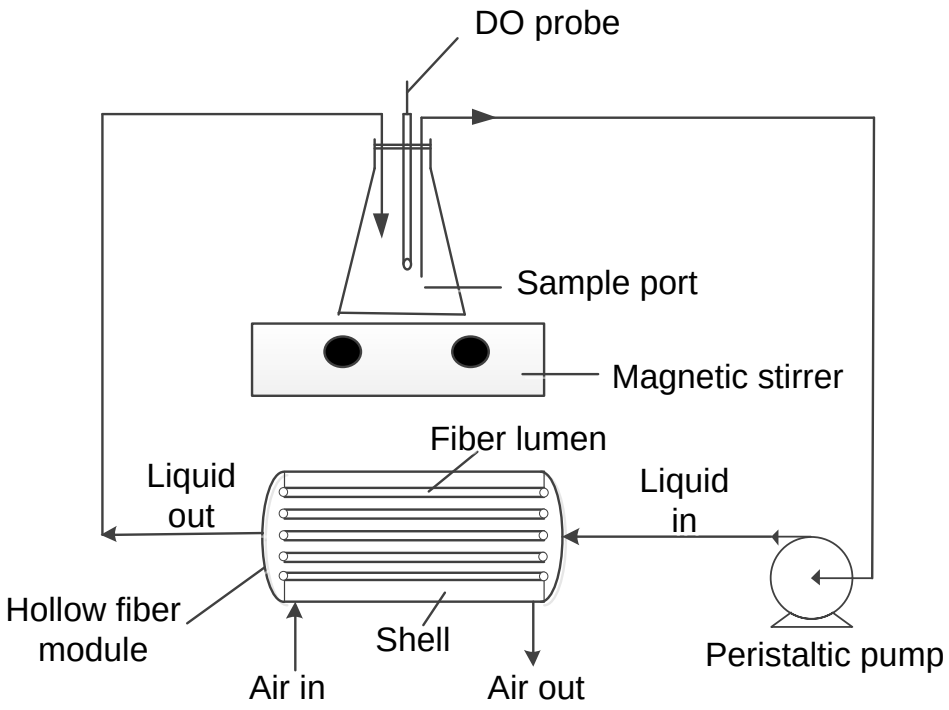

Figure 5.1. Experimental setup for hollow fiber module performance comparison to bubbling

The liquid used was de-ionized water. The liquid was recirculated through the sample port and back to the hollow fiber module using a Masterflex® Pump Controller 7553-60 (Cole-Parmer, Montreal, Quebec, Canada). For experiments done with 65mL of liquid, the sample port for the hollow fiber module was an in-house made glass tube of volume 15mL. A 100mL beaker (VWR, Mississauga, Ontario, Canada) was used for bubbling with 65mL of liquid. For experiments done with 225mL of liquid, the sample port was a 250mL Erlenmeyer flask (VWR). A 250mL Erlenmeyer flask (VWR) was used for bubbling with 225mL of liquid. A 1.5 inch magnetic stir bar (VWR) was used for agitation at 500RPM in the 250mL sample ports in some of the experiments. Air was supplied to the module and for bubbling at a flowrate of 320mL.min^{-1} from an air line

after passing through a PTFE 0.2 micron filter (VWR). Nitrogen (95%), (Praxair Canada, Mississauga, Ontario, Canada) was supplied at the same flowrate as air to sparge the system. The gas flow was countercurrent to the liquid flow in the membrane module. The orifice diameter for bubbling was 0.2cm. The flow-through module maintained the gas pressure at near atmospheric and below the bubble point of the membrane. The liquid was recirculated through the shell side of the module and alternately through the lumen side to compare the difference in configurations on the oxygen mass transfer. The dissolved oxygen (DO) concentration in liquid was measured with an Orion 081010MD polarographic dissolved oxygen probe (Thermo Scientific, Ottawa, Canada) connected to an Orion 3 star meter (Thermo Scientific). The probe was calibrated by saturating de-ionized water with air. A zero point calibration was also done by sparging de-ionized water with nitrogen. The liquid temperature was maintained at 24^{o}C.

5.1.3 Determination of $K_L a$

By measuring the DO concentration over time, $K_L a$, was determined using the dynamic method as described earlier in Chapter 3, Section 3.1.4. Only the air on trial was used after sparging to a near zero DO concentration with nitrogen. Each trial was done three times with the average value of the three air-on cycles plotted. The error was determined by dividing the standard deviation by the mean of the three trials.

5.1.4 Determination of approximate power input

The power input to the hollow fiber module was given by the following:

$$Pow = \frac{\Delta P}{\rho_L} \dot{m}_L \tag{5.1}$$

where *Pow* is the approximate power input to the system; ΔP is the liquid pressure drop across the module; ρ_L is liquid density; $\dot{m}_L$ is the mass flowrate of liquid. The liquid pressure drop at various liquid flowrates for the hollow fiber module was determined by an in-house manometer. The power input by bubbling was given by the following:

$$Pow = \frac{\Delta P}{\rho_a}\dot{m}_a \tag{5.2}$$

where ΔP is the pressure drop; ρ_a is the density of air; $\dot{m}_a$ is the mass flowrate of air. The pressure drop is equal to the hydrostatic head and was given by:

$$\Delta P = \rho_L g h \tag{5.3}$$

where g is the acceleration due to gravity; and h is the height that the bubbles have to travel through the liquid in the flask. In both cases, the power input, *Pow*, was divided by the reactor liquid volume used, V_L, to determine the approximate power input per reactor volume.

5.2 Results and Discussion

The microporous hollow fiber membrane module that was tested enabled oxygen transfer to the liquid compartment. $K_L a$ was calculated by measuring the dissolved oxygen concentration over time and the error for the three trials in each experiment was found to be within ±2.1% for liquid flow in the shell side and within ±1.9% for liquid flow in the lumen side of the hollow fiber module. The error in the bubbling trials was found to be within ±2.7%.

5.2.1 Effect of bubble free aeration on K_La with shell side liquid flow

The K_La for the 65mL volume of de-ionized water for bubble-free aeration in the hollow fiber module at various liquid recirculation rates on the shell side was determined and compared to bubbling under the same conditions. The results are depicted in Figure 5.2.

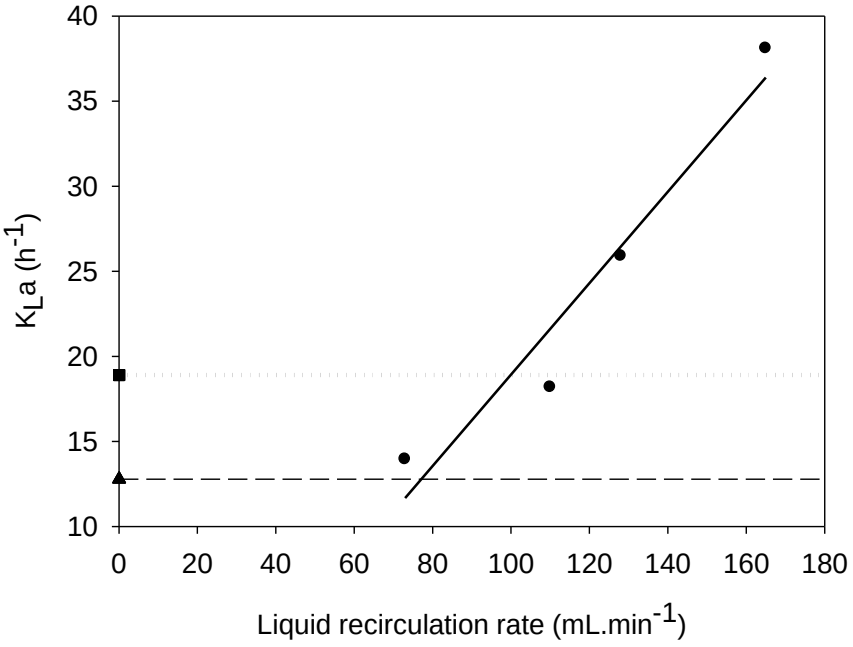

Figure 5.2. Effect of bubble free aeration on K_La with shell side liquid flow with liquid volume of 65mL de-ionized water. •Bubble-free aeration with shell side liquid flow; ■…Bubbling with 500 RPM stirring; ▲- - -Bubbling without stirring

It was observed that the K_La for bubble-free aeration increased almost linearly as the liquid flow around the fibers increased. This agrees well with the results from Chapter 3 and is explained by the reduction of the liquid boundary layer around the fibers as the

liquid flow is increased which causes less resistance to oxygen mass transfer. As expected, the K_La for bubbling increased when there was agitation in the sample port as better mixing was attained and larger bubbles were broken up into smaller ones thus increasing the interfacial area. The K_La for bubble-free aeration in shell side liquid flow surpassed that of bubbling (without stirring) at all liquid flowrates tested. However, only at a liquid recirculation rate of 128mL.min^{-1} and above did the K_La for bubble-free aeration surpass that of bubbling (with stirring) and was approximately double that of bubbling (with stirring) at a liquid recirculation rate of 165mL.min^{-1}. Higher liquid flow is necessary to reduce the resistance in the liquid boundary layer and promote better flow and transfer of dissolved oxygen in the media.

5.2.2 Effect of bubble free aeration with lumen side liquid flow on K_La

It was hypothesized that having the liquid flow inside the fibers as opposed to outside the fibers would increase K_La. To test this, the volume of the liquid used had to be increased from 65mL to 225mL. This was done because the dynamic of the dissolved oxygen electrode can only be considered negligible on the K_La values if 10 times the probe lag constant, 10τ, is less than the time characteristic for oxygen transport, $1/K_La$ (Garcia-Ochoa and Gomez, 2009). This condition would not be satisfied if the value of K_La was greater than 72h^{-1}, as the probe lag constant was determined to be 4.8 ± 0.2s from Section 3.2.2. Therefore the volume of the liquid tested was increased to accommodate this requirement to reduce the error in measurements.

The K_La for the 225mL volume of de-ionized water for bubble-free aeration in the hollow fiber module at various liquid recirculation rates was determined and compared to bubbling under the same conditions. The results are depicted in Figure 5.3.

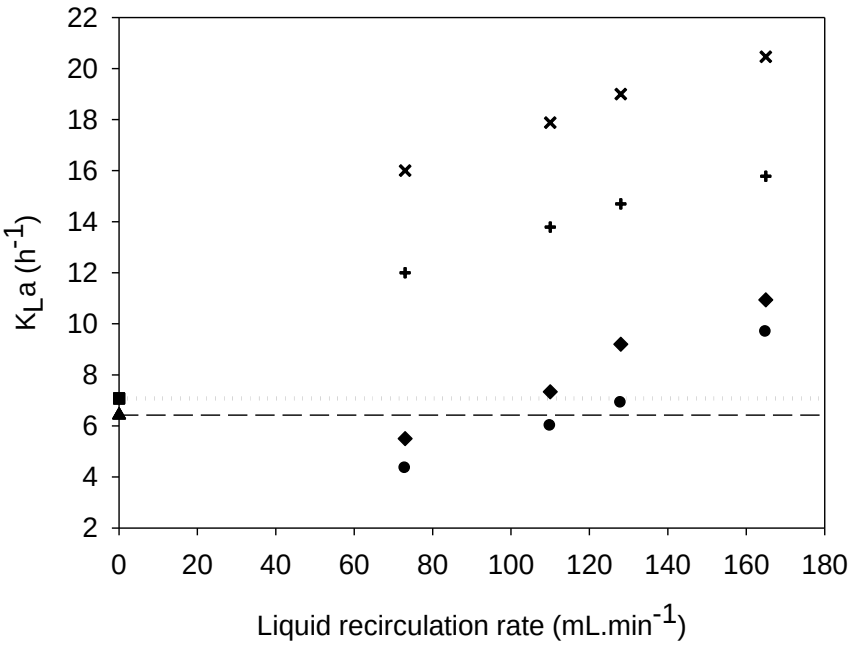

Figure 5.3. Comparison of K_La from bubble free aeration with lumen side and shell side liquid flow to bubbling with liquid volume of 225mL. x Bubble-free aeration with lumen side liquid flow with 500 RPM stirring; +Bubble-free aeration with lumen side liquid flow without stirring; •Bubble-free aeration with shell side liquid flow without stirring; ♦Bubble-free aeration with shell side liquid flow with 500 RPM stirring; ■…Bubbling with 500 RPM stirring; ▲- - -Bubbling without stirring

Having the liquid flow inside the fibers increased the K_La by approximately 2 times than having a shell side flow. Greater oxygen mass transfer was therefore observed when the liquid was recirculated in the lumen side of the module. This is partly due to the fact that

there is greater interfacial area and liquid velocity in the lumen side than the shell side of this module. The lower oxygen mass transfer in the shell side liquid flow is also the result of stagnant areas that developed between the fibers and other dead zones in the shell, which would reduce oxygen mass transfer. Increasing the liquid flow was found to increase the oxygen mass transfer in the shell side liquid flow as it also reduced the dead zones in the module. However, these results are specific to this type of module. Modifications can be made in module configuration to reduce this effect as dead zones can be limited by having better distribution of the fibers throughout the shell side if need be. The $K_L a$ for bubble-free aeration with liquid flow inside the fibers was found to be approximately 3 times higher than that of bubbling. Increased interfacial areas and reduced dead zones resulted in higher oxygen mass transfer than conventional bubbling. One potential disadvantage with recirculating the liquid through the fibers is that the pressure drop and power input will be higher than having a the liquid flow outside the fibers as significant pumping power is needed to force the liquid through the small diameters of the hollow fibers.

5.2.3 Comparison of power input by bubble-free aeration to bubbling

The approximate power input per reactor volume of the system was calculated for both bubbling and recirculating the liquid through the fibers for experiments with 225mL of de-ionized water according to Equations 5.1, 5.2 and 5.3. The results are depicted in Figure 5.4.

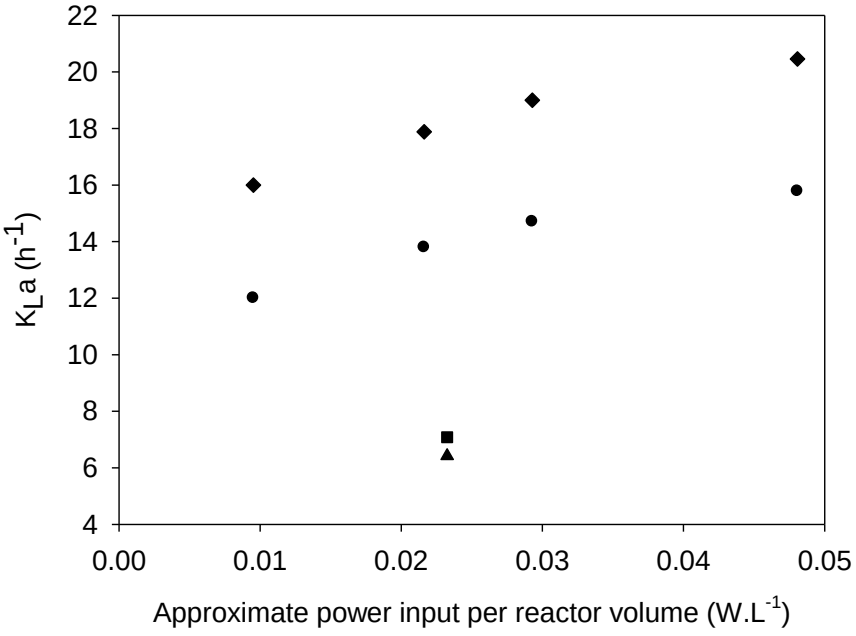

Figure 5.4. Effect of power input per reactor volume on $K_L a$ for bubbling and bubble-free aeration with liquid inside the fibers. ♦Bubble-free aeration with lumen side liquid flow with 500 RPM stirring; •Bubble-free aeration with lumen side liquid flow without stirring; ■Bubbling with 500 RPM stirring; ▲Bubbling without stirring

The power input required for pumping liquid through the hollow fiber modules increases as the liquid flowrate increases according to Equation 5.1. However it was found that even for power inputs lower than bubbling, the oxygen mass transfer was higher when bubble-free aeration with the hollow fiber module was used. At a slightly less power input to bubbling, the $K_L a$ was about 2-3 times higher when using bubble free-aeration than bubbling. This result is particularly beneficial for power generation processes like the Biogenerator where minimization of the energy input is a key aspect of optimization. Therefore, bubble-free aeration with hollow fiber membranes is a potential way of having

higher oxygen mass transfer and increased performance with a lower power input to the system. If the energy input is not major concern, as in the case of production of certain high value products, then the oxygen mass transfer can be increased significantly by using bubble-free aeration as opposed to bubbling by increasing the liquid flowrate.

5.2.4 Comparison of K_L from hollow fiber module and flat module

The K_L obtained from the hollow fiber module and the flat module (from Chapter 3, using polypropylene with pore size 0.45μm) was computed and compared to the approximate power input in each case for different recirculation and agitation rates. Methods and calculations are shown in the appendix (Section 10.3). The results are depicted in Figure 5.5.

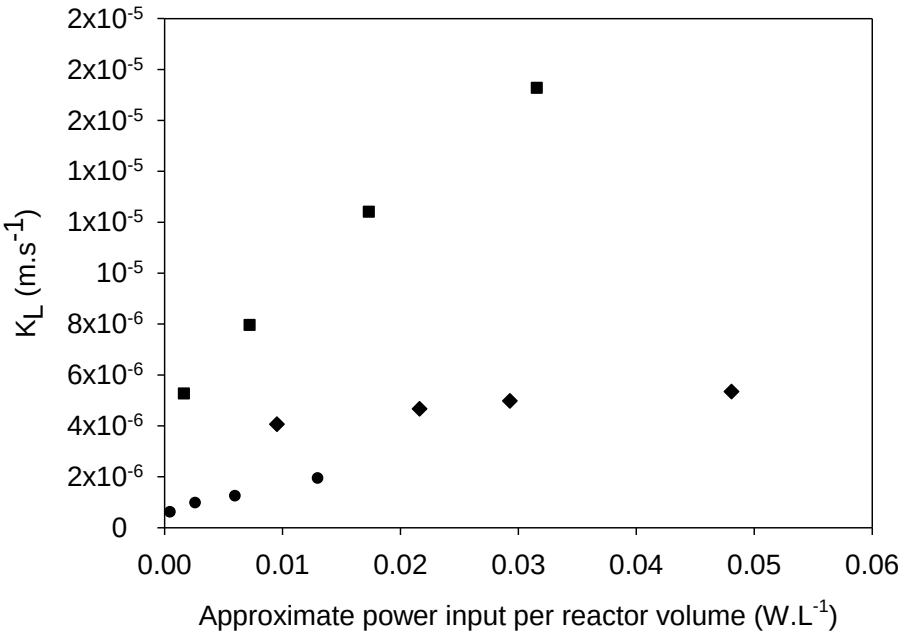

Figure 5.5. Comparison of K_L for hollow fiber and flat modules. •Hollow fiber module with shell side liquid flow; ♦hollow fiber module with lumen side liquid flow; ■flat membrane module

At relatively the same power input, the K_L for the flat module was higher than the hollow fiber module as there were more ideal flow conditions in the flat module due to less dead zones. Therefore, there is still potential to increase K_L in hollow fiber modules by improving module design and reducing dead zones which would result in greater oxygen mass transfer.

5.3 Hollow fiber bubble free-aeration with Bioreactor medium

Similar experiments were done with the setup and conditions specified in Section 5.1.2, but with 165mL of the bioreactor solution obtained from the Biogenerator instead of de-ionized water to determine the effect of bubble-free aeration for oxygen mass transfer using this liquid as compared to bubbling. The preparations and measurement methods of the bioreactor solution used was already described in Chapter 3 (Section 3.3).

5.3.1 Results and Discussion

The effects of bubble-free aeration with the hollow fiber module on the mass transfer coefficient of oxygen compared to bubbling is illustrated in Figure 5.6 when a bioreactor solution of pH 0.98 with 40g.L^{-1} Fe^{3+} and 0.56g. L^{-1} Fe^{2+} was used.

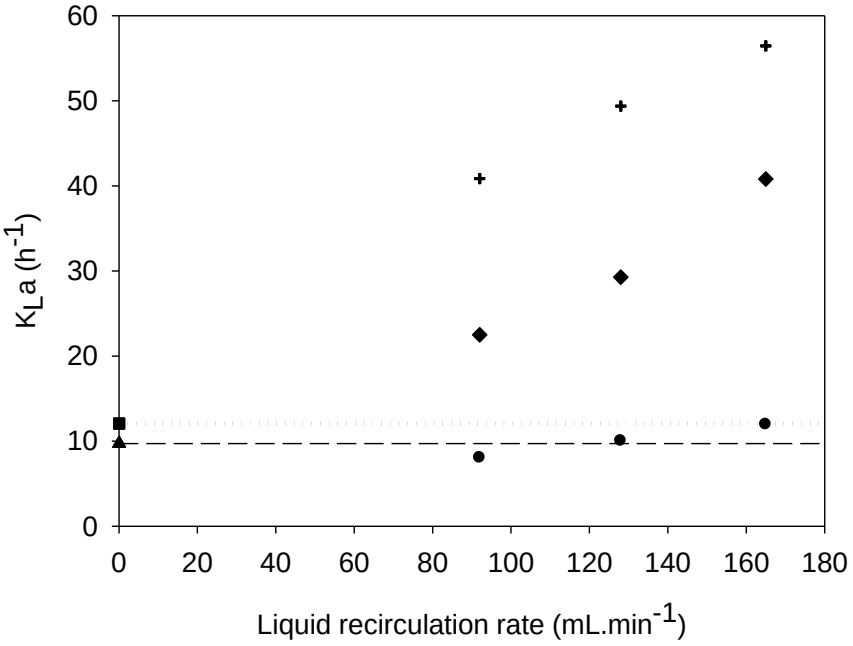

Figure 5.6. Comparison of K_La obtained by bubble-free aeration to bubbling in the bioreactor solution. +Bubble-free aeration with lumen side liquid flow with 500 RPM stirring; ♦Bubble-free aeration with lumen side liquid flow without stirring; ●Bubble-free aeration with shell side liquid flow without stirring; ■Bubbling with 500 RPM stirring; ▲ Bubbling without stirring

The error in K_La determination for the three trials in each experiment, obtained by dividing the standard deviation by the mean, was found to be within ±2.4% for liquid flow in the shell side and within ±2.2% for liquid flow in the lumen side of the hollow fiber module. The error in the bubbling trials was found to be within ±3.1%. Analogous with the results from using de-ionized water, bubble-free aeration with the bioreactor solution was found to have higher oxygen mass transfer when the liquid was recirculated inside of the fibers as opposed to outside due to the reduction of dead zones and higher

interfacial area. There was an almost linear increase in the oxygen mass transfer coefficient with increasing the liquid flowrate due to the reduction of the liquid boundary layer. In all cases of liquid recirculation rates tested, the K_La of bubble-free aeration with a lumen side liquid flow was higher than that of bubbling. The lowest lumen side liquid flow tested, which was 92 mL.min^{-1}, was found to have approximately 2.3 times greater K_La than bubbling without stirring and approximately 3.4 times greater K_La than bubbling with stirring in the sample port. This effect was enhanced by increasing the liquid flowrate and demonstrates the ability of bubble-free aeration to increase the oxygen mass transfer in bioreactors with this solution and ultimately increase the performance as more oxygen would be available for the *L. ferriphilum* to oxidize the ferrous irons.

5.3.1.1 Comparison of power input for bubbling and bubble-free aeration in the bioreactor solution

The approximate power input per reactor volume was calculated for both bubbling and recirculating the liquid through the fibers for experiments with 150mL of the bioreactor solution from the Biogenerator. The results are depicted in Figure 5.7.

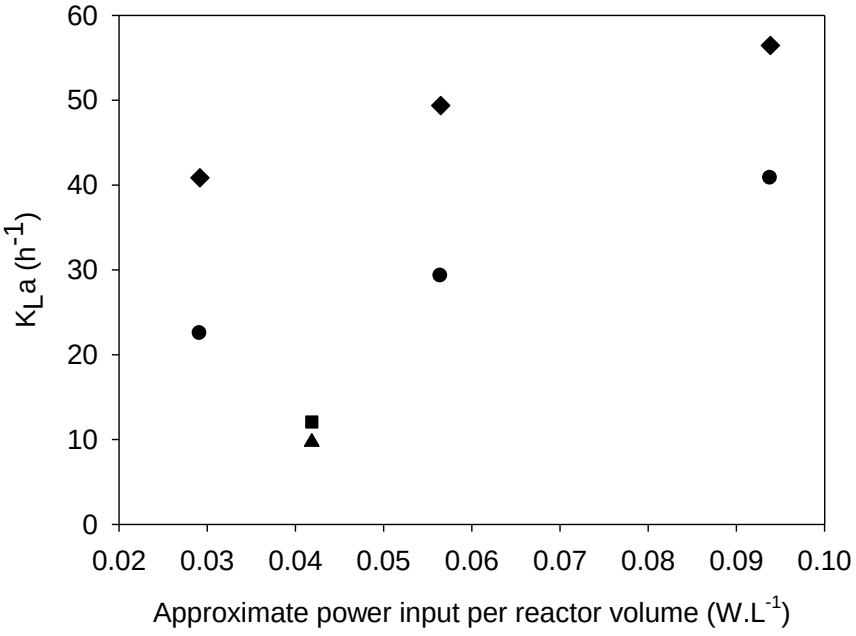

Figure 5.7. Effect of power input per reactor volume on $K_L a$ for bubbling and bubble-free aeration for the bioreactor solution with liquid inside the fibers. ♦Bubble-free aeration with lumen side liquid flow with 500 RPM stirring; •Bubble-free aeration with lumen side liquid flow without stirring; ■Bubbling with 500 RPM stirring; ▲Bubbling without stirring

Higher $K_L a$ values than bubbling were achieved at relatively the same or lower power input with lumen side liquid flow. Therefore, by using bubble-free aeration in the Biogenerator, higher $K_L a$ values can be achieved at lower power input in the bioreactor solution. Greater oxygen mass transfer would result in improved performance of the Biogenerator at a reduced energy input. This shows the potential of reducing cost as smaller volumes can be used to achieve the same or higher $K_L a$ as compared to bubbling. Bubble-free aeration has demonstrated its advantages over conventional bubbling in this system.

5.4 Conclusions from oxygen mass transfer in hollow fiber experiments

- Increasing the liquid flowrate for up to 165mL.min^{-1} in both the shell and the lumen sides of the hollow fiber module resulted in an almost linear increase in the oxygen mass transfer due to reduction in the liquid boundary layer on the fibers.
- Bubble-free oxygen mass transfer had higher K_La with lumen side liquid flow than shell side liquid flow due to increased interfacial areas and reduced dead zones.
- Lumen side liquid flow had approximately 3 times greater K_La than bubbling with agitation for de-ionized water.
- Shell side liquid flow had approximately 1.5 times greater K_La than bubbling with agitation for de-ionized water.
- Lumen side liquid flow was found to have higher K_La and a lower power requirement than bubbling, at a liquid flowrate of 110mL.min^{-1} and below for de-ionized water.
- Bubble-free aeration with lumen side liquid flow had significantly higher K_La than bubbling for the bioreactor solution from the Biogenerator with lower power input.

5.5 Nomenclature

g	acceleration due to gravity	$m.s^{-2}$
h	height of bubbles in liquid	m
K_La	volumetric mass transfer coefficient	h^{-1}
$\dot{m}_a$	mass flowrate of air	$kg.s^{-1}$
$\dot{m}_L$	mass flowrate of liquid	$kg.s^{-1}$
Pow	approximate power input to the system	W
ΔP	is the liquid pressure drop across the module	Pa
V_L	reactor liquid volume	m^3

Greek letters:

ρ_L	liquid density	$kg.m^{-3}$
ρ_a	density of air	$kg.m^{-3}$

Chapter 6 : Hollow fiber bubble-free CO_2 mass transfer

As proven in Chapter 4, the use of microporous membranes for bubble-free gas transfer is not gas specific/selective for the dissolved gases in this study. Therefore the same hollow fiber module tested for oxygen mass transfer should give similar relationships with carbon dioxide mass transfer. More efficient carbon dioxide mass transfer is a key goal in the photoautotrophic cultivation of microalgae as better growth rates can be achieved at lower energy input and less carbon dioxide will be released to the atmosphere. Bubble-free gas transfer with microporous hollow fiber modules has the potential of having higher mass transfer rates than bubbling due to higher interfacial areas.

The main goals of this chapter are to determine the volumetric mass transfer coefficient, K_La, for bubble-free carbon dioxide gas transfer with a hollow fiber module at various liquid flowrates and compare this to bubbling under the same conditions. The effect of recirculating the liquid in the shell side of the module and in the lumen side will also be investigated to compare the difference in performance.

6.1 Materials and Methods

The Liqui-Cel® 1 x 5.5 MiniModule® (Membrana, Charlotte, NC, USA) was used with properties as described in Section 5.1.1 and a similar experimental setup from Section 5.1.2 of Chapter 5. Carbon dioxide gas (Praxair Canada, Mississauga, Ontario, Canada) was supplied at a flowrate of 200mL.min^{-1} using high precision rotameters (Omega, Stamford, CT, USA). The gas flow was countercurrent to the liquid flow. The dissolved carbon dioxide concentration was measured according to Section 4.1.2 and the volumetric

mass transfer coefficient, K_La, was determined according to Section 4.1.3 of Chapter 4. The liquid used was de-ionized water with 10% vol. of a carbon dioxide buffer solution ISE-8750-R1 (Omega), to maintain the pH of the liquid at 4.89 for the probe to efficiently measure dissolved carbon dioxide. The liquid volume used was 150mL. Three trials were done for each experiment and the mean value of K_La was plotted.

6.2 Results and Discussion

The microporous hollow fiber membrane module that was tested enabled carbon dioxide mass transfer to the liquid. K_La was calculated by measuring the dissolved oxygen concentration over time and the error was found to be within ±2.5% for shell side liquid flow and ±2% for lumen side liquid flow. The error in the bubbling experiments was found to be within ±2.9%.

The K_La for bubble-free carbon dioxide gas transfer in the hollow fiber module at various liquid recirculation rates in the shell and the liquid sides was determined and compared to bubbling under the same conditions. The results are depicted in Figure 6.1.

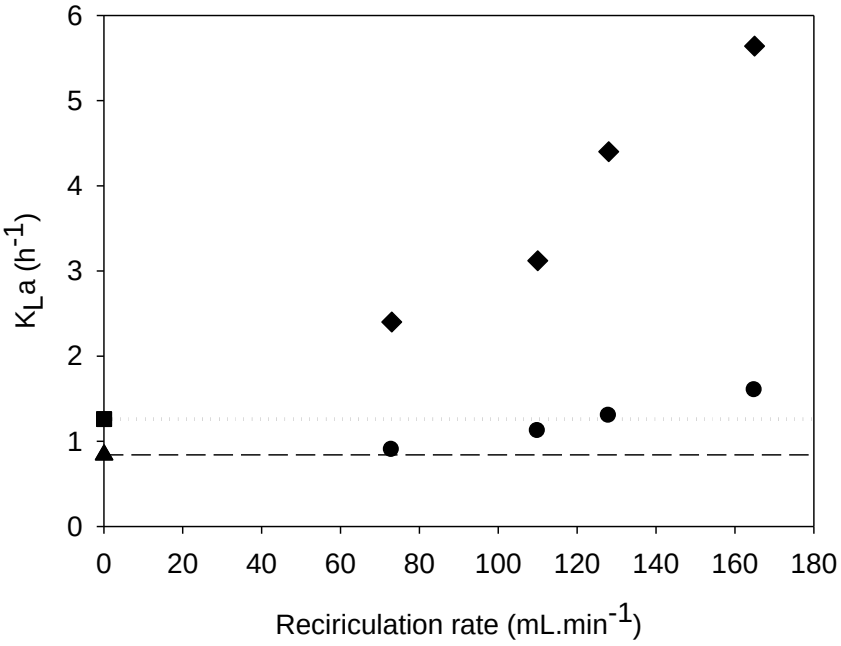

Figure 6.1. Comparison of bubble-free carbon dioxide gas transfer from a hollow fiber module to bubbling. ♦Bubble-free gas transfer with lumen side liquid flow with 500RPM stirring; • Bubble-free gas transfer with shell side liquid flow with 500RPM stirring; ■Bubbling with 500 RPM stirring; ▲Bubbling without stirring

Similar relationships were observed with bubble-free carbon dioxide gas transfer in the hollow fiber module. The K_La increased as the liquid recirculation rate increased in both cases in the module due to the reduction in the liquid boundary layer. Having the liquid flow in the lumen side resulted in greater carbon dioxide mass transfer as dead zones in the liquid compartment of the module was limited and higher interfacial areas was utilized. The K_La was found to be approximately 4.5 times greater than bubbling when lumen side liquid flow was used in the hollow fiber module, and about 1.3 times greater than bubbling when shell side liquid flow was used at the highest liquid flowrate tested

with agitation in the sample ports. This demonstrates the potential of hollow fibers to increase the carbon dioxide mass transfer in bioreactors and the potential for incorporating its use into photobioreactors for micro-algal cultivation.

6.3 Conclusions from bubble free carbon dioxide mass transfer

- Bubble-free carbon dioxide mass transfer, exhibited similar relationships as oxygen mass transfer.
- Increasing the liquid flowrate for up to for up to 165mL.min^{-1} in both the shell and the lumen sides of the hollow fiber module increased the carbon dioxide mass transfer due to reduction in the liquid boundary layer on the fibers.
- Lumen side liquid flow had approximately 4.5 times greater K_La than bubbling with agitation.
- Shell side liquid flow had approximately 1.3 times greater K_La than bubbling with agitation.

Chapter 7 : Cultivation of microalgae: bubbling versus bubble-free

Improving phtotobioreactor design to obtain more efficient carbon dioxide transfer and better light distribution is a critical goal for the optimization of phototrophic cultivation of microalgae. The supply of carbon dioxide to microalgal cultures in closed systems during photoautotrophic cultivation is most conventionally done by bubbling. Better carbon dioxide mass transfer to the culture would result in improved growth and less carbon dioxide released to the atmosphere.

Hollow fiber membranes have the potential to achieve higher carbon dioxide mass transfer rates than bubbling with minimal carbon dioxide loss to the atmosphere (Kumar et al., 2010) Also, the oxygen produced during photosynthesis can be removed by the membranes and result in lower toxicity of the growth media. Previous researchers have postulated that the growth of *Nannochloropsis sp.* was not significantly improved by a hollow fiber module (Carvalho and Malcata, 2001). However they used a relatively low lumen side liquid flow of 28mL.min^{-1} which resulted in a large residence time of 235s for algal cells inside the fibers without light. Higher liquid flowrates would be beneficial as we have shown in Chapter 6 that carbon dioxide mass transfer is increased by increasing the liquid flowrate and this would also result in a lower residence time and more light exposure to the culture.

Flat plate photobioreactors have also been shown to have better growth rates than conventional bubble columns as better light distribution can be achieved in the growth

media as the light intensity decreases exponentially with an increase in both the distance from the reactor wall and cell concentration. This is represented by the following (Chen et al., 2011):

$$\frac{I_L}{I_o} = \exp(-\gamma L) \qquad (7.1)$$

where I_L is the light intensity, at a depth of L; I_o is the original light intensity; and γ is the turbidity. Thin plated photobioreactors can be stacker vertically to obtain better light penetration than in traditional bubble columns. Gentler aeration can be achieved with the use of membranes for bubble-free aeration in flat plate photobioreactors.

Bubble-free aeration has several other advantages over bubbling for cultivation of microalgae. There would be less shear stress which would result in lower cell death compared to bubbling. A lower gas pressure is needed and potentially a lower power input depending on the liquid flowrate used, as it does not have to overcome the hydrostatic head as in bubbling. Decreasing nozzle size in bubbling would result in greater carbon dioxide mass transfer however this is known to lead to greater shear stress on the cells and more death (Barbosa et al., 2004).

The main goals of this chapter is to evaluate the growth rates of cultivation of *Chlorella vulgaris* by bubble-free aeration in a hollow fiber module and in a novel flat membrane module, and compare them to conventional bubbling in a flask.

7.1 Material and methods

7.1.1 Microalga strain and culture medium

The media used was Modified Bold's media with properties shown in Table 7.1.

Table 7.1. Modified Bold's media preparation properties

Component	Concentration in stock solution ($g.L^{-1}$ H_2O)	Amount used per liter of media (ml)
Macronutrients		
$NaNO_3$	25	10
$MgSO_4.7H_2O$	7.5	10
$CaCl_2.2H_2O$	2.5	10
K_2HPO_4	7.5	10
KH_2PO_4	17.5	10
NaCl	2.5	10
Alkaline solution		1
Na_2EDTA	63.9	
KOH	552.5 ml of 1M KOH	
Acidified Iron Solution		1
$FeSO_4.7H_2O$	4.98	
H_2SO_4	1 ml	
Boron solution		1
H_3BO_3	11.42	
Trace metal solution		1
$ZnSO_4.7H_2O$	8.82	
$CuSO_4.5H_2O$	1.57	
$MnCl_2.4H_2O$	1.44	

The cell culture used in this study was *C. vulgaris* UTEX 2714 (UTEX, Austin, TX, USA). A 1:5 volume ratio of a slightly concentrated *C. vulgaris* sample to media was

prepared and added to each setup during inoculation. A total volume of 450mL was batch cultivated for 17 days in each of the three photobioreactor setups.

7.1.2 Experimental setup

The experimental setup is depicted in Figure 7.1.

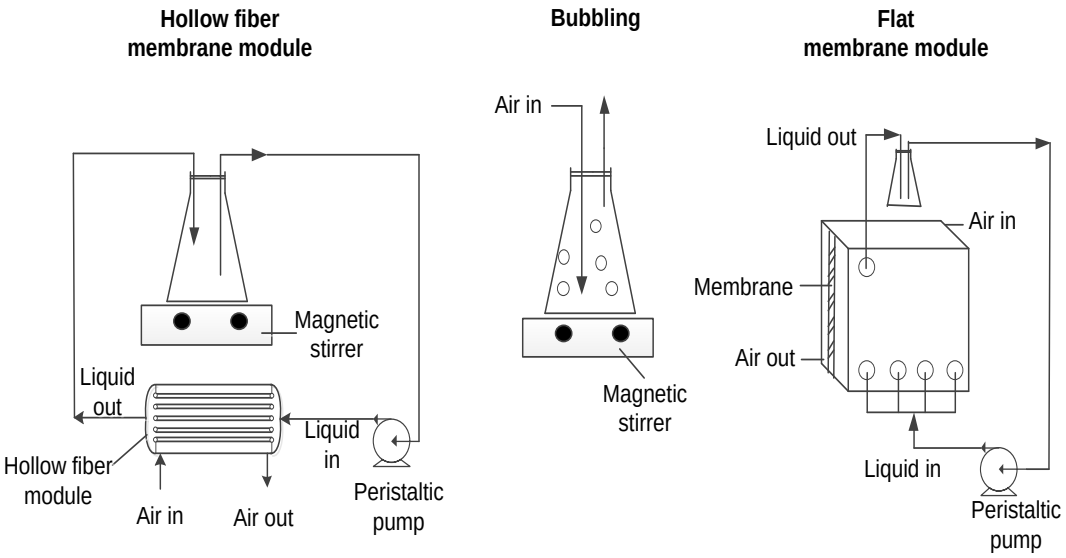

Figure 7.1. Experimental setup for cultivation of *C. vulgaris*

Each setup was exposed to two fluorescent Philips Plant and Aquarium bulbs at 1600 Lux for 12 hour on-off cycles. Air was used as the gas in each setup and maintained at a flowrate of 250mL.min^{-1} using high precision rotameters (Omega, Stamford, CT, USA) after passing through a PTFE 0.2 micron filter (Cole-Parmer, Montreal, Quebec, Canada).

For the hollow fiber photobioreactor, the module used was the Liqui-Cel® 1 x 5.5 MiniModule® (Membrana, Charlotte, NC, USA) with polypropylene as the membrane material and properties as already described in Section 5.1.2 of Chapter 5. The liquid was

recirculated a rate of 110mL.min^{-1} through the lumen side of the fibers to a 500mL Erlenmeyer flask (VWR, Missisauga, Ontario, Canada). The gas flow was countercurrent to the liquid flow. The liquid in the flask was agitated at 200RPM with a PTFE coated magnetic stir bar (VWR).

A novel flat membrane module was fabricated from Plexi glass with a liquid compartment length of 14.7cm, height of 14.7cm and width of 1.3cm. A flat sheet Polypropylene membrane (Sterlitech, Kent, WA, USA) with pore size 0.1µm was used as the gas-liquid contactor. The effective membrane surface area was 216cm^2. The gas compartment contained unique vertical ridges spaced equally at 0.5cm apart to act as a membrane support against the hydrostatic pressure. The gas flow was countercurrent to the liquid flow. The liquid was recirculated to a 125mL sample flask (VWR) at a flowrate of 200mL.min^{-1}.

A 500mL Erlenmeyer flask (VWR) was used as the third photobioreactor with the liquid being agitated at 200RPM with a PTFE coated magnetic stir bar (VWR). A nozzle opening of 2mm was used to supply the air into the liquid.

7.1.3 Cell concentration determination

Three 10µl samples were taken from each setup approximately every two days. The cell count was determined using a Haemocytometer 3200 (Hausser Scientific Company, Horsham, PA, USA). The microscope used was a Leica CME microscope (Leica Microsystems CMS GmbH, Wetzlar, Germany). The total number of cells counted in the 1mm^2 grid of the haemocytometer was multiplied by 10^4 to get the concentration in number of cells.mL^{-1}. Concentrated samples were diluted with de-ionized water and the

cell count was multiplied by the dilution factor to determine the sample concentration. The mean value and the standard deviation of the three samples were plotted.

7.1.4 Growth rate determination

The specific growth rate in the exponential phase for each setup was determined according to the following:

$$ln\,(X) = \mu\, t + ln(X_o) \qquad (7.2)$$

where X is the cell concentration; μ is the specific growth rate; t is the time; and X_o is the initial cell concentration. By plotting $ln(X)$ versus t, μ can be determined from linear regression of the exponential phase and compared for each setup.

7.2 Results and Discussion

By measuring the cell concentration over time, the comparison of photoautotrophically cultivated *C. vulgaris* in each setup is depicted in Figures 7.2 and 7.3.

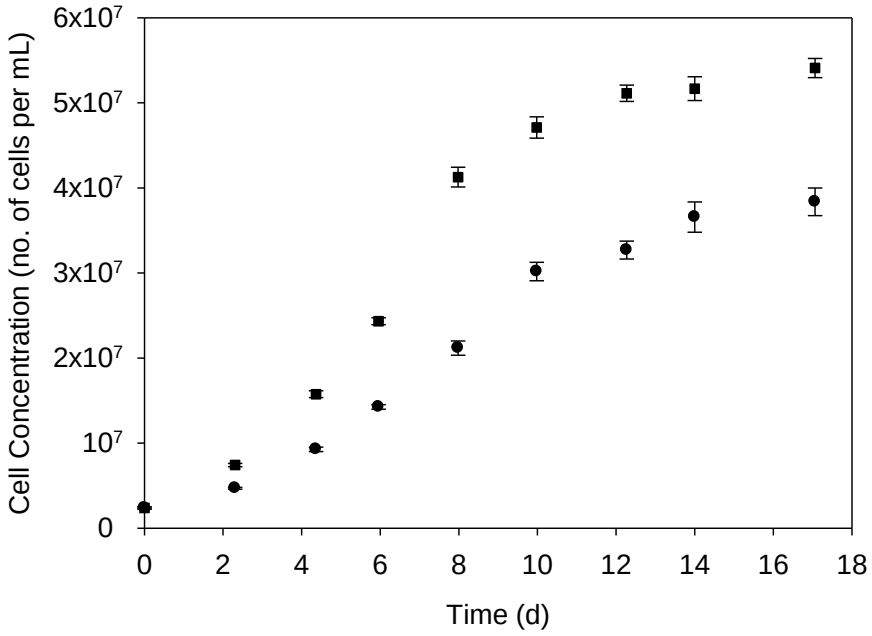

Figure 7.2. Effect of bubble-free aeration in the flat membrane module and bubbling on growth of *C. vulgaris*. •Bubbling; ■Flat membrane module

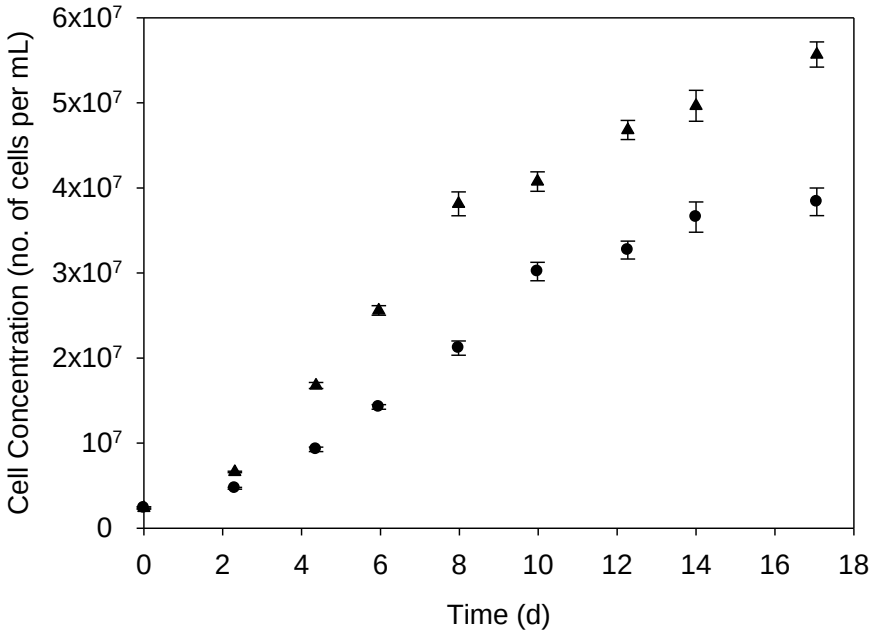

Figure 7.3. Effect of bubble-free aeration in the hollow fiber membrane module and bubbling on growth of *C. vulgaris*. •Bubbling; ▲Hollow fiber membrane module

The culture grew well in each of the setups tested under similar conditions. Better growth was achieved with bubble-free aeration in the flat membrane module and the hollow fiber module as compared to bubbling. This is shown in Table 7.2.

Table 7.2. Specific growth rates for *C. vulgaris* in each setup studied

Photobioreactor	μ (d^{-1})
Flat membrane module	0.393
Hollow fiber module	0.386
Flask	0.280

As show earlier in Chapter 6, more efficient carbon dioxide mass transfer can be achieved in the hollow fiber module when compared to bubbling. Using bubble free aeration in the hollow fiber module resulted in a higher growth rate and greater final cell concentration than bubbling as more carbon was available to the *C. vulgaris* for utilization. The residence time in the hollow fiber module was 8.7 seconds. Increasing the liquid flowrate inside the fibers may result in even higher growth as greater mass transfer rates can be achieved and less time spent without light.

The specific growth rate in the flat membrane module was found to be similar to the hollow fiber module and greater than bubbling. The final cell concentration was also higher than that of bubbling. As both light and carbon dioxide are limiting during photoautotrophic cultivation of microalgae, the flat membrane module offered better light penetration and distribution to the culture according to Equation 7.1. The thickness of the liquid in the flat membrane module was significantly less than the thickness in the 500mL flasks used in both bubbling and in the hollow fiber module. As the concentration of cells increased, more light was available to the culture in the flat module than in the flasks which resulted in higher growth than bubbling. This flat module has several advantages as it can be easily scaled up and has relatively low cost.

7.3 Conclusions from bubble-free cultivation of microalgae

- Bubble-free aeration had similar growth rates in the hollow fiber module and the novel flat membrane module.

- Better light penetration was achieved with the novel flat membrane module and better carbon dioxide mass transfer was achieved with the hollow fiber membrane module.
- Bubble-free aeration had approximately 1.4 times greater growth rate that conventional bubbling under the same conditions.
- Higher cell final concentrations were achieved with bubble-free aeration than bubbling for the growth of *C. vulgaris* under the same conditions.

7.4 Nomenclature

I_L	light intensity	$W.m^{-2}$,
I_o	original light intensity	$W.m^{-2}$
L	depth of reactor	m
t	time of growth	d
X	cell concentration	no. of cells per mL
X_o	initial cell concentration	no. of cells per mL.

Greek letters:

γ	liquid turbidity	NTU
μ	specific growth rate	d^{-1}

Chapter 8 : Summary of work

The overall hypothesis that bubble-free oxygen and carbon dioxide mass transfer using microporous membranes can provide more efficient mass transfer than conventional bubbling was generally satisfied.

8.1 Conclusions

The major conclusions from this research are:

- The gas mass transfer rate increased as the degree of hydrophobicity of the membranes increased in the flat membrane module.
- Hydrophobic membranes had higher K_L than hydrophilic membranes in the flat membrane module.
- Surprisingly, it was found out that the mass transfer coefficient in the case when a gas and liquid are separated by a hydrophobic membrane is larger than in the case of a direct gas-liquid contact and lower when separated by a hydrophilic membrane.
- Increasing liquid agitation or flow resulted in an almost linear increase for hydrophobic membranes tested in the flat membrane module and the hollow fiber module.
- The effect of pore size on gas mass transfer was negligible for the hydrophobic membranes.
- The thickness of the liquid boundary layer is the main limiting factor for bubble-free gas mass transfer.

- Similar relationships were observed for both oxygen and carbon dioxide mass transfer which proves that microporous membranes are not gas specific/selective when being used as gas-liquid contactors for low soluble gases in water.
- Liquid properties influence the overall gas mass transfer rate.
- Greater oxygen and carbon dioxide mass transfer were observed with lumen side liquid flow than shell side liquid flow in the hollow fiber module.
- The lumen and shell side liquid flow had approximately 3 times and 1.5 times greater oxygen mass transfer respectively, than bubbling in de-ionized water.
- Higher oxygen mass transfer coefficients were achieved for lumen side liquid flow at a lower power input compared to bubbling in both de-ionized water and the bioreactor solution.
- Better growth of *C. vulgaris* was observed when using bubble-free aeration in both the hollow fiber module and the novel flat membrane module than compared to conventional bubbling. The specific growth rate increased by approximately 1.4 times.

8.2 Recommendations

Based on the results presented, recommendations for future work include:

- Fabrication and testing of superhydrophobic microporous membranes to be used as gas-liquid contactors for bubble-free gas transfer. We have shown that the increase in hydrophobicity results in an increase in gas mass transfer. These will have to be tested for long term usage and stability.
- Evaluation of long term stability of the hollow fiber module for oxidation of ferric irons by the *L. ferriphillum* in the bioreactor solution. The performance of bubble-

free aeration versus bubbling can be compared to determine which method provides better oxidation over a long period of time and potentially test in a mini bio-fuel cell. Better oxidation rates will lead to improved fuel cell performance.

- Evaluation of growth rates of microalgae with shell-side liquid flow. This configuration also has potential for better growth as the shell material is transparent and more light will be available to the culture as opposed to lumen side liquid flow. However the gas mass transfer is lowered with this configuration but the liquid flowrate can be increased to address this issue. Having the gas flow through the fibers would also result in less condensation as water vapour would be immediately swept through.
- Fabrication and comparison of growth rates of microalgae using a bubble-free aeration in a hollow fiber module incorporated with a flat plate module. As we have shown the effect on growth rate with the increased carbon dioxide mass transfer in the hollow fiber module, and the improved light distribution in the flat membrane module, combining both can potentially result in higher growth rates as both carbon dioxide and light are limiting in the phototrophic cultivation of microalgae.

9 Bibliography

Ahmed, T., Semmens, M., J., 1992. Use of sealed end hollow fibers for bubbles membrane aeration: experimental studies. Journal of Membrane Science 69, 1-10.

Ahmed, T., Semmens, M., J., 1992. The use of independently sealed microporous hollow fiber membranes for oxygenation of water: model development. Journal of Membrane Science 69, 11-20.

Ahmed, T., Semmens, M., J., Voss, M., A., 2004. Oxygen transfer characteristics of hollow-fiber, composite membranes. Advances in Environmental Research 8, 637-646.

Aptel, P., Semmens, M., J., 1996. Multiphase Membrane Processes, in: American Water Works Association Research Foundation, Lyonanaise des Eaux, Water Research Commission of South Africa. (Eds.), Water treatment membrane processes. Mc-Graw Hill, New York, pp 8.1-8.19.

Baker, R., W., 2004. Membrane Technology and Applications, second ed. Wiley, New Jersey.

Barbosa, M., J., Hadiyanto, Wijffels, R., H., 2004. Overcoming shear stress of microalgae cultures in sparged photobioreactors. Biotechnology and Bioengineering 85 (1), 78–85.

Blanch, H., W., Clark, D., S., 1997. Biochemical Engineering. Marcel Dekker, Ney York.

Brindle, K., Stephenson, T., Semmens, M, J., 1999. Pilot-Plant Treatment of a High-Strength Brewery Wastewater Using a Membrane-Aeration Bioreactor. Water Environment Research 71 (6), 1197-1204.

Carvalho, A., P., Malcata, X., F., 2001. Transfer of Carbon Dioxide within Cultures of Microalgae: Plain Bubbling versus Hollow-Fiber Modules. Biotechnology Progress 17, 265-272.

Cheng, L., Zhang, L., Chen, H., Gao, C., 2006. Carbon dioxide removal from air by microalgae cultured in a membrane-photobioreactor. Separation and Purification Technology 50, 324–329.

Chen, C., Yeh, K., Aisyah, R., Lee, D., Chang., J., 2011. Cultivation, photobioreactor design and harvesting of microalgae for biodiesel production: A critical review. Bioresource Biotechnology 102 (1), 71-81.

Chern, J., Yang, S., 2004. Measuring and Modeling of Oxygen Transfer Rate in a Drop. Industrial & Engineering Chemistry Research 43, 7657-7663.

Chisti, Y., 2007. Biodiesel from Microalgae. Biotechnology Advances 25 (3), 294- 306.

Cote, P., Bersillon, J., Huyard, A., Faup G., 1988. Bubble-free aeration using membranes: process analysis. Journal (Water Pollution Control Federation) 60 (11), 1986-1992.

Cote, P., Bersillon, J., Huyard, A., Faup G., 1989. Bubble-free aeration using membranes: mass transfer analysis. Journal of Membrane Science 47, 91-106.

Duan, C., Luo, M., Yang, C., Jiang, H., Xing, X., 2010. Effects of Different Hollow Fiber Membrane Modules on Bubbleless Aeration of Methane and Oxygen. The Chinese Journal of Process Engineering 10 (2), 395-399.

Ferreira,B., S., Fernandes,H., L., Reis, A., Mateus, M., 1998. Microporous Hollow Fibres for Carbon Dioxide Absorption: Mass Transfer Model Fitting and the Supplying of Carbon Dioxide to Microalgal Cultures. Journal of Chemical Technology and Biotechnology 71, 61-70.

Franz, J., A., Williams, R., J., Joseph, Flora, J., R., V., Meadows, M., E., Irwin, W., G., 2002. Electrolytic oxygen generation for subsurface delivery: effects of precipitation at the cathode and an assessment of side reactions. Water Research 36, 2243–2254.

Garcia-Ochoa, F., Gomez, E., 2009. Bioreactor scale-up and oxygen transfer rate in microbial processes: An overview. Biotechnology Advances 27, 153–176.

Garcia-Ochoa, F., Gomez, E., Santos,V.,E., Merchuk, J.,C., 2010. Oxygen uptake rate in microbial processes: An overview, Biochemical Engineering Journal 49, 289–307.

Gillot, S., Capela-Marsal, S., Roustan, M., He´duit, A., 2005. Predicting oxygen transfer of fine bubble diffused aeration systems—model issued from dimensional analysis. Water Research 39, 1379–1387.

Harun, R., Singh, M., Forde, G., M., Danquah, M., K., 2010. Bioprocess engineering of microalgae to produce a variety of consumer products. Renewable and Sustainable Energy Reviews 14, 1037–1047.

IUPAC, 1985. Reporting physisorption data for gas/solid systems with special reference to the determination of surface area and porosity. Pure and Applied Chemistry 57 (4), 603-619.

Karamanev D., 2009. Biofuel cell. US Patent number: 7572546B2.

Karamanev, D., G., Pupkevich, V., R., Hojjatti, H., 2010. Bio-fuel cell system. International patent application number: PCT/CA2010/001210.

Kies, F., K., Benadda, B., Motterbein, M., 2004. Experimental study on mass transfer of a co-current gas–liquid contactor performing under high gas velocities. Chemical Engineering and Processing 43 (11), 1389-1395.

Kreulen, H., Smolders, C. A. , Versteeg, G. F., Van Swaaij, W. P. M., 1993. Determination Of Mass Transfer Rates In Wetted And Non-Wetted Microporous Membranes. Chemical Engineering Science 48 (11), 2093-2102.

Kumar, A., Yuan, X., Sahu, A., K., Dewulf, J., Ergasa, S.,J.,Van Langenhoveb, H., 2010. A hollow fibermembrane photo-bioreactor for CO2 sequestration from combustion gas coupled with wastewater treatment: A process engineering approach. Journal of Chemical Technology and Biotechnology 85, 387–394.

Li., N., N., Fane, A., G., Ho, W., S., W., Matsuura, T., 2008. Advanced Membrane Technology and Applications. Wiley, New Jersey.

Lv, Y., Yu, X., Jia, J., Tu, S., Yan, J., Dahlquist E., 2011. Fabrication and characterization of superhydrophobic polypropylene hollow fiber membranes for carbon dioxide absorption. Applied Energy 90 (1), 167-174.

Matsuoka, H., Fukada, S., Toda, K., 1992. High Oxygen Transfer Rate in a New Aeration System Using Hollow Fiber Membrane. Biotechnology and Bioengineering 40, 346-352.

Patwardhan, A., W., 2003. Rotating Biological Contactors: A Review. Industrial & Engineering Chemistry Research 42, 2035-2051.

Penev, K., 2010. Kinetics of Iron Oxidation by Leptosprillum ferriphilum, Ph.D. Thesis, UWO, London, Canada.

Philichi, T., L., Stenstrom, M., 1989. Effects of Dissolved Oxygen Probe Lag on Oxygen Transfer Parameter Estimation. Journal (Water Pollution Control Federation) 61 (1), 83-86.

Pupkevich V., 2007. Electrochemical Aspects of the Biogenerator, M.E.Sc. Thesis, UWO, London, Canada.

Quere, D., 2002. Rough ideas on wetting. Physica A 313, 32-46.

Ralph T.,R., Hogarth M.,P., 2002. Catalysis for low temperature fuel cells. Platinum Metals Review, 46, 117-135.

Sadoff, H., L., Halvorson, H., O., Finn R., K., 1956. Electrolysis as a means of aerating submerged cultures of microorganisms. Applied Microbiology 4, 167-170.

Schlichting, H., 1979. Boundary-Layer Theory, seventh ed. McGraw-Hill, New York.

Semmens, M., J., 2008. Alternative MBR configurations: using membranes for gas transfer. Desalination 231, 236-242.

Spolaore, P., Joannis-Cassan, C., Duran, E., Isambert, A., 2007. Commercial Applications of Microalgae. Journal of Bioscience and Bioengineering 101 (2), 87-96.

Vasel, J., L., Schrobiltgen, P., 1991. Oxygen transfer in trickling filters. Water Research 25 (1), 53-60.

Voss, M., A., Ahmed, T., Semmens, M., J., 1999. Long-Term Performance of Parallel-Flow, Bubbleless, Hollow-Fiber-Membrane Aerators. Water Environment Research 71 (1), 23-30.

Wilk, T., 2003. Trickling filters and biofilm reactor modelling. Reviews in Environmental Science and Bio/Technology 2, 193–212.

Winter, C., 2005. Into the hydrogen energy economy-milestones. International Journal of Hydrogen Energy 30, 681-685.

Xue, C., Jia, S., Zhang, J., Ma, J., 2010. Large-area fabrication of superhydrophobic surfaces for practical applications: an overview. Science and Technology of Advanced Materials 11 (3), 1-15.

Zhang, W., Li, J., Chen, G., You, W., Jiang, Y., Sun, W., 2010. Experimental Study of Mass Transfer in Membrane Absorption Process Using Membranes with Different Porosities. Industrial Engineering and Chemistry Research 49, 6641–6648.

Zoueshtiagh, F., Alley, R., Colley, A., J., Thomas, P., J., Carpenter, P., W., 2003. Laminar-turbulent boundary layer transition over a rough rotating disk. Physics of Fluids 15 (8), 2441-2444.

10 Appendix

10.1 Chapter 3 Sample data and calculations

Hydrophobicity measurements

The following figure illustrates one sample of the contact angle obtained for the PTFE 0.22µm membrane using de-ionized water.

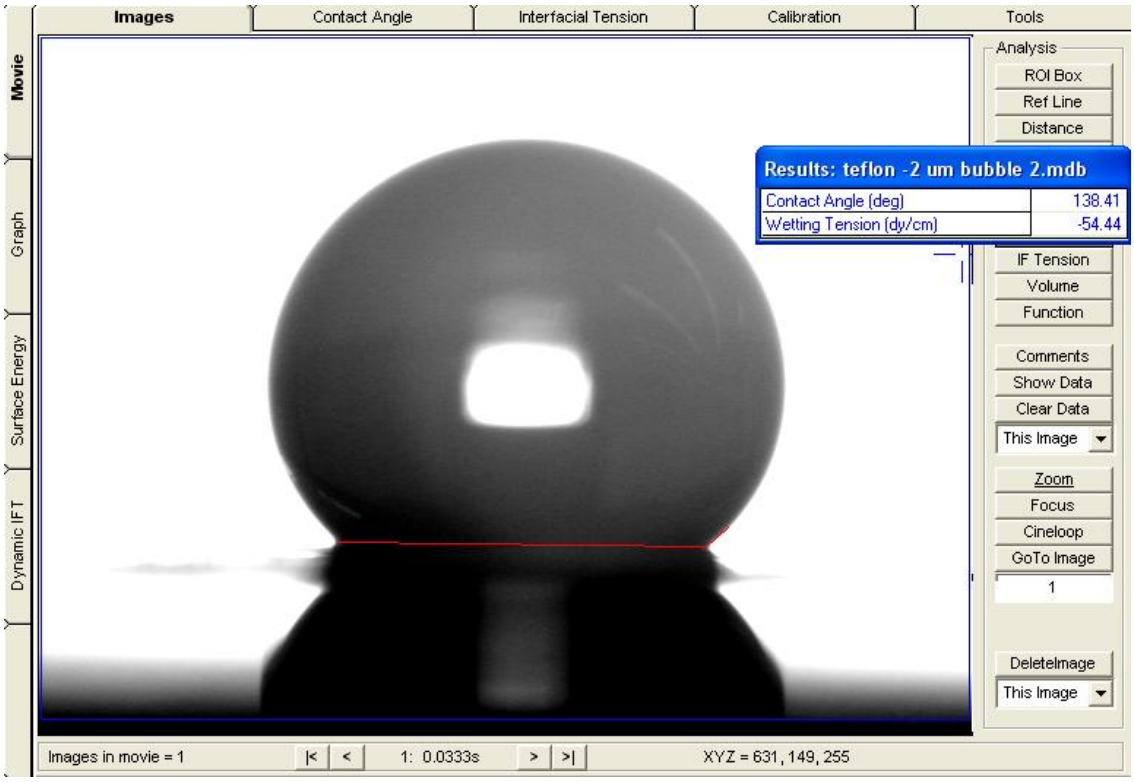

This was repeated for 5 trials for each membrane sample tested and the mean value plotted with the standard deviation.

Determination of K_L

The following data was obtained by measuring the dissolved oxygen concentration over time during the oxygen mass transfer in de-ionized water in the flat membrane module with a polypropylene membrane of pore size 0.1µm and agitation of 700 RPM.

Time (min)	[DO] ($mg.L^{-1}$)	$\ln[(C^*-C)/(C^*-C_o)]$
0	1.26	0.000
1	1.56	-0.043
2	2.02	-0.113
3	2.43	-0.179
4	2.80	-0.243
5	3.17	-0.311
6	3.50	-0.376
8	4.08	-0.502
9	4.32	-0.560
10	4.56	-0.620
11	4.76	-0.674
12	4.97	-0.733
13	5.17	-0.793
14	5.32	-0.841
15	5.50	-0.901
16	5.65	-0.954
17	5.80	-1.010
18	5.94	-1.066
20	6.16	-1.159
24	6.58	-1.367
26	6.76	-1.471
28	6.89	-1.554
30	7.05	-1.666

By plotting $ln[(C^*-C)/(C^*-C_o)]$ versus time, the slope was found to be equal to -0.0578min^{-1} which is the equal to the value of $-K_La$. The interfacial area, a, was calculated by:

$a = S_M / V_L$ = 8.04cm^2/ 10.6 mL

= 0.7588cm^{-1}

$K_L = K_La / a$

= 0.0578min^{-1}/ 0.7588cm^{-1} x (1min/60s) x (1m/100cm)

= 1.269 x10^{-5} m.s^{-1}.

This procedure was repeated for all other trials in K_L determination.

Calculation of liquid velocity

For the flat membrane module it was assumed that the liquid velocity was equal to the tip velocity of the stirrer which was calculated by:

$U = N * 2 * \pi * (d_{stir} / 2)$

Where N is the agitation rate and d_{stir} is the diameter of the stirrer.

U = 600 rpm (1min/60s) * 2 * π *(0.0127m / 2)

U= 0.399m.s^{-1}

This was repeated for the remaining agitation rates.

10.2 Chapter 4 Sample data and calculations

Probe calibration

The following calibration curve was obtained for the dissolved carbon dioxide probe to convert the mV readings to ppm CO_2.

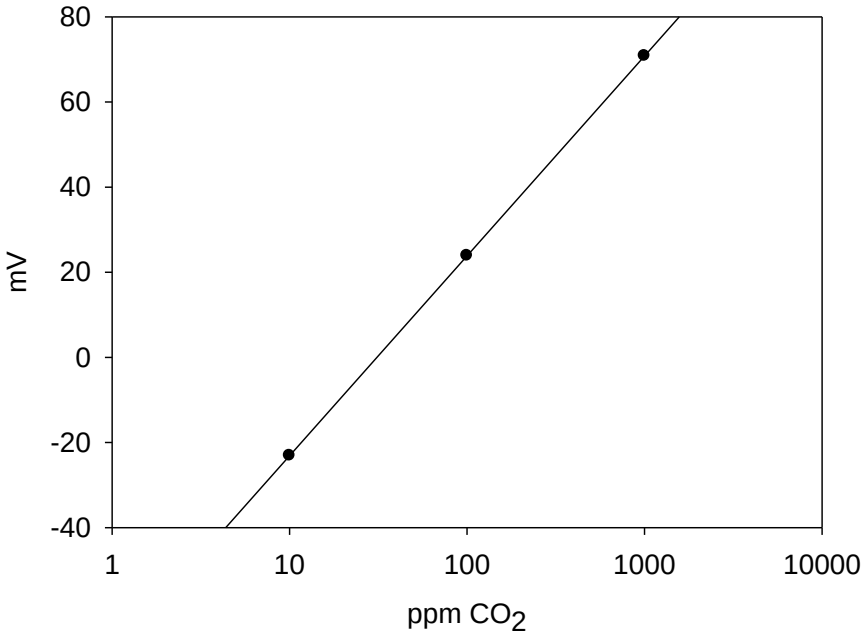

By linear regression it was found that, y = 20.39ln(x) – 70.05. The mV values from the meter were converted to ppm CO_2 values using this equation.

Determination of K_L

The following data was obtained by measuring the dissolved carbon dioxide concentration over time during the carbon dioxide mass transfer in de-ionized water with 10% vol. carbon dioxide buffer solution in the flat membrane module with a 0.45μm

polypropylene membrane and agitation of 900 RPM. The value of C* was found to be 1375ppm in this liquid at 24^{o}C.

Time	mV	ppm	ln(C*-C/C*-C_o)
0	-40.4	4.281	0.000
1	-3.6	26.02	-0.016
2	18.1	75.43	-0.053
3	31.6	146.2	-0.109
4	40.2	222.9	-0.174
5	46.0	296.3	-0.24
6	50.4	367.7	-0.308
7	53.8	434.4	-0.377
8	56.5	495.9	-0.444
9	58.6	549.8	-0.507
10	60.5	603.4	-0.575
11	62.1	652.7	-0.641
12	63.4	695.7	-0.702
14	65.6	774.9	-0.826
16	67.2	838.2	-0.937
18	68.4	888.9	-1.037
20	69.4	933.7	-1.133
22	70.4	980.6	-1.246
24	71.0	1010	-1.323
26	71.9	1055	-1.456
28	72.4	1082	-1.542
30	72.9	1109	-1.638
35	74.2	1182	-1.958

By plotting $ln[(C^*-C)/(C^*-C_o)]$ versus time, the slope was found to be equal to -0.055min^{-1} which is the equal to the value of $-K_La$. The interfacial area, a, was previously calculated to be 0.7588cm^{-1}

$K_L = K_La / a$

$= 0.055\text{min}^{-1} / 0.7588\text{cm}^{-1} \times (1\text{min}/60\text{s}) \times (1\text{m}/100\text{cm})$

$= 1.208 \times 10^{-5}\ \text{m.s}^{-1}$.

This procedure was repeated for all the other trials in this chapter.

10.3 Chapter 5 Sample data and calculations

Determination of K_La

The following data was obtained by measuring the dissolved oxygen concentration over time during the oxygen mass transfer with the bioreactor solution in the hollow fiber membrane module with a shell side liquid flow of 128mL.min^{-1}. The value of C* was found to be 7.6mg.L^{-1} in this liquid at 24^{o}C.

Time (s)	[DO] (mg/L)	ln(C*-C/C*-Co)
0	1.50	0.000
15	1.81	-0.052
30	2.06	-0.096
45	2.29	-0.139
60	2.50	-0.179
75	2.70	-0.219
90	2.94	-0.269
105	3.12	-0.309
120	3.30	-0.350
150	3.62	-0.427
180	3.94	-0.511
210	4.21	-0.587
240	4.46	-0.664
300	4.88	-0.808

By plotting $ln[(C^*-C)/(C^*-C_o)]$ versus time, the slope was found to be equal to -0.167min^{-1} which is the equal to the value of $-K_La$.

K_La = 0.167min^{-1}x (60min/1h)

$K_L a$ = 10.02h^{-1}.

This procedure was repeated for all other trials for $K_L a$ determination.

Calculation of K_L in the hollow fiber module

The value of K_L for shell side liquid flow of 165 mL.min^{-1} of de-ionized water was calculated from:

$a = S_m / V_L$

a = [2* π *(3 x 10^{-4} m / 2)*0.116m*2300] / (2.25 x $10^{-4}m^{-3}$)

a= 1117.7m^{-1}

$K_L = K_L a / a$

K_L = 7.68 h^{-1} / 1117.7m^{-1} *(1h / 3600s)

K_L = 1.91 x 10^{-6} m.s^{-1}.

Similar calculations were done for remaining recirculation flowrates and for the lumen side liquid flow.

Calculation of liquid velocity in the hollow fiber module

The liquid velocity for shell side liquid flow of 165 mL.min^{-1} was calculated according to the following (Aptel and Semmens, 1996):

$U = 4\,Q / [\pi\,(d_s^2 - n*d_f^2)]$

where U is the liquid velocity; Q is the liquid volumetric flowrate; d_s is the shell diameter; d_f is the fiber outer diameter; and n is the number of fibers.

$U = 4\ (2.75 \times 10^{-6}\ m^3.s^{-1}) / [(\pi\ ((0.0254m)^2 - (2300*(300 \times 10^{-6}\ m)^2))]$

$U = 7.99 \times 10^{-3}\ m.s^{-1}$

Power calculations

The following is an example of the power calculations used in Chapter 5. The approximate power input per volume for de-ionized water in the hollow fiber module at a lumen side liquid flowrate of $110mL.min^{-1}$ was calculated as followed:

$Pow = (\Delta P * \dot{m}_L) / \rho_L$

$= (2646.7Pa * 0.001833\ kg.s^{-1}) / 997kg.m^{-3}$

$= 0.004866W$

$Pow / V_L = 0.004866W / 0.225L$

$= 0.0216W.L^{-1}$.

Similar calculations were done for the power input for the bioreactor solution whose density was found to be $1200kg.m^{-3}$ and also for shell side liquid flow in the hollow fiber module.

The following procedure was used to determine the approximate power input per volume in the flat membrane module from Chapter 3 (using polypropylene with pore size 0.45

μm) at an agitation of 300 RPM and was also applied to the agitation rates of 500, 700 and 900 RPM.

The Reynolds number was calculated by:

$$Re = N D_i^2 \rho / \mu$$

Where Re is the Reynolds number, N is the agitation rate, D_i is the stirrer diameter, ρ is the liquid density and, μ is the liquid viscosity.

$$Re = (300\text{RPM} / 60\ \text{s.min}^{-1}) * (0.0127\text{m})^2 * (997\ \text{kg.m}^{-3}) / (8.9 * 10^{-4}\ \text{Pa.s})$$

$$Re = 906$$

For each Reynolds number at various agitation speeds, the Power number, P_N, was determined from a figure of Power number versus Reynolds number using a propeller as an estimation (Blanch and Clark, 1997). The power was calculated according to:

$$P_N = P / \rho N^3 D_i^5$$

where P is the power input in Watts.

$$P = P_N \rho N^3 D_i^5$$

$$P = (0.42) * (997) * (300/60)^3 * (0.0127)^5 = 1.73 \times 10^{-5}\ \text{W}.$$

$$P / V_L = 1.73 \times 10^{-5}\ \text{W} / 0.0106\text{L} = 1.64 \times 10^{-3}\ \text{W.L}^{-1}$$

Curriculum Vitae

Name: Ravi Balgobin

Post-secondary Education and Degrees:

Western University
London, Ontario, Canada
2005-2010 B.E.Sc.
Graduated with Distinction

Western University
London, Ontario, Canada
2010-2012 M.E.Sc. Candidate

Honours and Awards:

Ontario Graduate Scholarship
2011-2012

1st Place at the 13th CSChE Ont-Que Biotechnology Conference
Oral Presentation: Oxygen mass transfer by bubble-free aeration using flat microporous membranes. 2011

2nd Place at the CBE Research Bridges Symposium
Oral Presentation: Bubble-free aeration using flat microporous membranes. 2011

Related Work Experience:

Graduate Teaching Assistant
Western University
2010-2012

Graduate Research Assistant
Western University
2010-2012

Publications:

Balgobin, R., Karamanev, D. (2012). Basic study of the Gas-Liquid Oxygen Mass Transfer by Bubble-free aeration. Chemical Engineering Science, paper submitted.

Balgobin, R., Garcia, B., Glibin, V., Karamanev, D. (2010). Preparation and proton conductivity of composite SiO2/ Poly (2- hydroxyethyl methacrylate) gel membranes. Solid State Ionics, 181, (31), 1403-1407.

Conference Proceedings:

Balgobin, R., Bassi, A., Karamanev, D. 2011. Bubble-free Carbon Dioxide Mass Transfer for Cultivation of Microalgae. Proc. 61st CSChE Conference, London, Ontario.

Balgobin, R., Karamanev, D. 2011. Bubble-free Oxygen Mass Transfer in Bioreactors by using Microporous Membranes. Proc. 61st CSChE Conference, London, Ontario.

Balgobin, R., Karamanev, D. 2011. Oxygen mass transfer by bubble-free aeration using flat microporous membranes. Proc. 13th CSChE Ontario-Quebec Biotechnology Meeting, Kingston, Ontario.

Related Extracurricular Activities

Social Programs and Tours Director
16th annual CSChE Conference
Western University
2010-2011

President
Chemical Engineering Club
Western University
2009-2010